Title
Autophagy induction enhances TDP43 turnover and survival in neuronal ALS models

Journal
Nature Chemical Biology, 10(8)

ISSN
1552-4450

Authors
Barmada, SJ
Serio, A
Arjun, A
et al.

Publication Date
2014

DOI
10.1038/nchembio.1563

Peer reviewed

nature chemical biology

ARTICLE

PUBLISHED ONLINE: 29 JUNE 2014 | DOI: 10.1038/NCHEMBIO.1563

Autophagy induction enhances TDP43 turnover and survival in neuronal ALS models

Sami J Barmada[1–3], Andrea Serio[4–6], Arpana Arjun[1], Bilada Bilican[4,5], Aaron Daub[1], D Michael Ando[1,7], Andrey Tsvetkov[1,8], Michael Pleiss[9], Xingli Li[3], Daniel Peisach[3], Christopher Shaw[10], Siddharthan Chandran[4,5] & Steven Finkbeiner[1,2,7,9,11–14]*

Amyotrophic lateral sclerosis (ALS) and frontotemporal dementia (FTD) have distinct clinical features but a common pathology—cytoplasmic inclusions rich in transactive response element DNA-binding protein of 43 kDa (TDP43). Rare TDP43 mutations cause ALS or FTD, but abnormal TDP43 levels and localization may cause disease even if TDP43 lacks a mutation. Here we show that individual neurons vary in their ability to clear TDP43 and are exquisitely sensitive to TDP43 levels. To measure TDP43 clearance, we developed and validated a single-cell optical method that overcomes the confounding effects of aggregation and toxicity and discovered that pathogenic mutations shorten TDP43 half-life. New compounds that stimulate autophagy improved TDP43 clearance and localization and enhanced survival in primary murine neurons and in human stem cell–derived neurons and astrocytes harboring mutant TDP43. These findings indicate that the levels and localization of TDP43 critically determine neurotoxicity and show that autophagy induction mitigates neurodegeneration by acting directly on TDP43 clearance.

ALS and FTD are fundamentally connected[1]. Neuronal and glial cytoplasmic accumulations of TDP43 occur in most ALS cases and the most common form of FTD (FTLD-TDP)[2], and mutations in several genes cause ALS, FTD or both[1]. TDP43 is a nuclear RNA-binding protein involved in several aspects of RNA processing[3] that actively shuttles between the nucleus and cytoplasm[4]. In ALS and FTLD-TDP, TDP43 is excluded from the nucleus[2], but such cytoplasmic mislocalization is common in neuronal injury or stress[5,6], and TDP43-positive inclusions may represent secondary pathology in some neurodegenerative disorders[7].

Over 30 mutations in the TDP43 gene (*TARDBP*) cause familial ALS (fALS) and FTLD-TDP[8]. We previously demonstrated that *TARDBP* mutations promote cytoplasmic TDP43 mislocalization and that mutant TDP43-induced neurodegeneration could be explained by cytoplasmic TDP43 toxicity[9]. Cytoplasmic accumulations of wild-type (WT) TDP43 are pathognomonic for sporadic ALS (sALS) and FTLD-TDP[2], and elevated TDP43(WT) levels are neurotoxic in multiple systems[10,11], linking abnormal protein homeostasis with sALS and fALS. Despite the potential importance of TDP43 metabolism to neuronal survival, prior studies were limited to cell lines or non-neuronal cell types[12,13], leaving open the possibility that neuron-specific differences in protein metabolism[14,15] underlie their susceptibility to TDP43-dependent pathology.

TDP43 accumulates when the ubiquitin-proteasome system or autophagy is inhibited[16,17], but it is unclear which is primarily responsible for clearing TDP43. Conflicting data suggest that autophagy can accelerate or slow disease progression. Although autophagy induction with rapamycin exacerbates neurodegeneration in transgenic ALS mice[18], genetically upregulating autophagy enhances survival in the same animals[19]. Rapamycin was beneficial in FTLD-TDP transgenic mice[20], but despite the effects of this and other mammalian target of rapamycin (mTOR) inhibitors in non-neuronal cells, their ability to induce neuronal autophagy per se is limited[14,21,22], and their off-target effects might affect disease activity in an autophagy-independent manner[23]. Careful pharmacodynamic studies confirming the autophagy-inducing effects of rapamycin and its derivatives in the central nervous system are often lacking or, when performed, fail to demonstrate autophagy induction[21]. In the few cases where autophagy has been clearly induced, the mechanism by which this pathway affects disease pathogenesis remains obscure as autophagy has broad effects on mitochondrial turnover, energy balance and global protein catabolism[23].

Using a structure-activity assay, we assembled a neuronal autophagy-inducing pharmacophore, used it to discover new autophagy inducers and then investigated the therapeutic potential of autophagy induction in a neuronal model of ALS. Stimulating neuronal autophagy enhanced TDP43 clearance and improved neuronal survival, and the changes in TDP43 turnover explained much of the survival benefit of autophagy induction, providing mechanistic insight into how autophagy mitigates TDP43-induced neurodegeneration.

RESULTS

TDP43 toxicity is dose dependent

We fused WT and ALS-associated mutant TDP43 ($TDP43^{A315T}$) (ref. 24) to enhanced GFP (EGFP) and transfected primary rodent

[1]Gladstone Institute of Neurologic Disease, San Francisco, California, USA. [2]Department of Neurology, University of California–San Francisco Medical Center, San Francisco, California, USA. [3]Department of Neurology, University of Michigan, Ann Arbor, Michigan, USA. [4]Euan MacDonald Centre for Motor Neurone Disease Research, University of Edinburgh, Edinburgh, Scotland, UK. [5]Medical Research Council Centre for Regenerative Medicine, University of Edinburgh, Edinburgh, Scotland, UK. [6]Departments of Materials and Bioengineering, and Institute for Biomedical Engineering, Imperial College, London, UK. [7]Biomedical Sciences Graduate Program, University of California–San Francisco, San Francisco, California, USA. [8]Department of Neurobiology and Anatomy, University of Texas Medical School, Houston, Texas, USA. [9]Keck Program in Brain Cell Engineering, Gladstone Institutes, San Francisco, California, USA. [10]Institute of Psychiatry, King's College London, London, UK. [11]Department of Physiology, University of California–San Francisco, San Francisco, California, USA. [12]Taube-Koret Center for Neurodegenerative Disease Research, San Francisco, California, USA. [13]Hellman Family Foundation Alzheimer's Disease Research Program, San Francisco, California, USA. [14]Roddenberry Stem Cell Program, San Francisco, California, USA. *e-mail: sfinkbeiner@gladstone.ucsf.edu

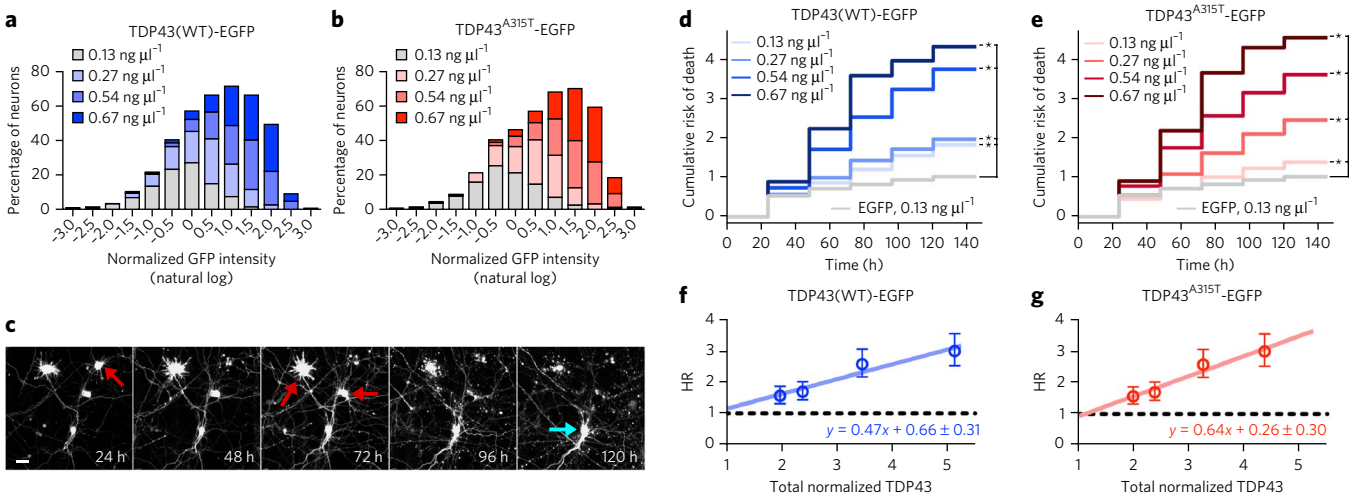

Figure 1 | The toxicity of TDP43 depends strongly on dose. (**a**,**b**) Histograms of TDP43(WT)-EGFP (**a**) and TDP43^{A315T}-EGFP (**b**) levels in individual neurons. Increasing amounts of DNA significantly shifted the distribution of log-transformed expression levels toward higher values ($P < 0.01$ for all comparisons, two-sided Kolmogorov-Smirnov test). TDP43(WT)-EGFP, $n = 1,287$ neurons, with 290–342 cells per group; TDP43^{A315T}-EGFP, $n = 1,290$, with 315–332 neurons per group. Values were pooled from 12 wells per condition, with experiments performed in duplicate. (**c**) Automated fluorescence microscopy. Primary rodent cortical neurons were transfected with mApple and TDP43-EGFP, and survival was determined by repeated imaging at regular intervals. The last time at which the cell was noted to be alive (red arrows) was used as the time of death. Cells that survive the entire length of the experiment (cyan arrow) were censored. Scale bar, 25 µm. (**d**,**e**) Cumulative risk of death over time for neurons transfected with EGFP, TDP43(WT)-EGFP (**d**) or TDP43^{A315T}-EGFP (**e**). **Supplementary Table 1** lists the number of neurons, hazard ratios, 95% CI and *P* values for each condition, as determined by Cox proportional hazards analysis. Results were pooled from 12 wells per condition, with experiments performed in duplicate. (**f**,**g**) Linear regression of calculated hazard ratio (± s.e.m.) as a function of total TDP43(WT)-EGFP ($R^2 = 0.9353$) (**f**) or TDP43^{A315T}-EGFP ($R^2 = 0.9574$) (**g**) level. The total TDP43 level was determined by quantitative immunocytochemistry using TDP43-specific antibodies (**Supplementary Fig. 3**) and normalized to the amount of TDP43 in nontransfected neurons. Dashed lines, reference (HR = 1).

cortical neurons with different amounts of construct and mApple, a survival and morphology marker (**Supplementary Results**, **Supplementary Fig. 1**). To determine TDP43-EGFP levels for each neuron, we measured single-cell fluorescence by automated fluorescence microscopy (AFM)[9,25]. Transient transfection with 0.13 ng µl^{-1} DNA gave a broad distribution of expression levels (**Fig. 1a**,**b**). Increasing the amount of DNA right-shifted the distribution, with more cells exhibiting higher TDP43-EGFP levels. We thus created specific populations of neurons expressing WT or mutant TDP43-EGFP at defined 'doses'.

To assess the relationship between TDP43 dose and survival, we determined the risk of death for neurons expressing WT and mutant TDP43-EGFP by longitudinal AFM (**Fig. 1c**). AFM measures the lifespan of individual neurons and gauges the impact of prespecified factors on the risk of death. Criteria for cell death in these assays—loss of mApple fluorescence or disruption of cell integrity—are more sensitive than conventional measures[25]. We calculated risk of death for each population of neurons through Cox hazards analysis, resulting in a hazard ratio (HR) analogous to relative risk in human clinical trials. Risk of death increased steadily with levels of TDP43(WT)-EGFP and TDP43^{A315T}-EGFP (**Fig. 1d**,**e** and **Supplementary Table 1**). WT and mutant TDP43 increased risk of death by 25–50% at low doses and ~300% at higher levels. For a given expression level, TDP43 was more toxic than other disease-associated proteins (data not shown), including fused-in-sarcoma (FUS) in fALS[1] or mutant huntingtin (Htt) in Huntington's disease[25]. In contrast, we noted no relationship between neuronal survival and EGFP levels (**Supplementary Fig. 2a**), suggesting a specific dose-dependent toxicity of TDP43.

We next used immunocytochemistry to determine total TDP43 levels in transfected neurons (**Supplementary Fig. 3a–e**). Neurons receiving 0.13 ng µl^{-1} DNA exhibited twice the endogenous TDP43 (en-TDP43) level, and those given 0.67 ng µl^{-1} DNA had fivefold more. We observed downregulation of en-TDP43 in several neurons (**Supplementary Fig. 3f**), but downregulation and survival were unrelated. For instance, downregulation was most efficient at the lowest dose of TDP43(WT)-EGFP (0.13 ng µl^{-1}; **Supplementary Fig. 3f**), but toxicity was maximal at the highest (0.67 ng µl^{-1}; **Fig. 1d**), consistent with *in vivo* studies showing no relation between en-TDP43 levels and disease[26]. In contrast, HR and TDP43 levels were linearly related (**Fig. 1f**,**g**): the risk of death increased 47% for every fold change in TDP43(WT)-EGFP levels and 64% for every fold change in TDP43^{A315T}-EGFP levels. Thus, even small increases in WT and mutant TDP43 can drive toxicity.

Measuring TDP43 clearance *in situ*

If TDP43 levels are directly proportional to neurodegeneration, augmenting TDP43 clearance might have therapeutic potential. The half-life of en-TDP43 in primary rodent cortical neurons by metabolic pulse chase (MPC) was 18 h (95% confidence interval (CI), 13.4–29.3 h; **Fig. 2a**,**b** and **Supplementary Fig. 4a**), longer than that observed in fibroblasts or immortalized cell lines (4–12 h)[12,13]. We suspected that this discrepancy might be due to cell type–specific differences in TDP43 stability or might be an artifact of the method used to measure half-life.

MPC is a population-based assay and is therefore susceptible to several potential confounds, including protein aggregation and cell death (**Fig. 2c**). To circumvent these, we developed a complementary *in situ* method for measuring TDP43 half-life (**Fig. 2d** and **Supplementary Fig. 4b**). Optical pulse labeling (OPL) uses photoconvertible proteins, such as Dendra2 (ref. 27), that irreversibly switch their spectral properties when exposed to short-wavelength light. We tagged TDP43(WT) with Dendra2 and expressed the construct in rodent primary cortical neurons and then photoconverted with 405-nm light. Neurons were imaged by AFM, and the data were analyzed in a population-based manner, as with MPC. Neurons were prospectively tracked and excluded after an aggregate was identified, and single-cell red fluorescence intensities

were summed to generate a population total and were normalized to the total immediately after photoconversion. TDP43(WT)-Dendra2 half-life measured by OPL (18 h, 95% CI, 15.1–23.4 h; **Fig. 2e**) was similar to en-TDP43 half-life as measured by MPC (**Fig. 2b**). These results have two important implications. First, overexpression and Dendra2 fusion do not affect TDP43 turnover. Second, OPL and MPC provided the same estimate of TDP43 half-life when the data were analyzed in an equivalent fashion, suggesting that both techniques measure the same biological processes acting on TDP43.

We wondered whether the results accurately reflected TDP43 clearance. At least two potential confounds are relevant to these measurements: cellular toxicity and protein aggregation (**Fig. 2c**). However, their respective contributions have previously been impossible to determine. With OPL, for what is to our knowledge the first time, we can directly measure the contributions of each to half-life estimations. For protein aggregation, we analyzed all cells, regardless of whether they exhibited visible inclusions. In doing so, TDP43(WT)-Dendra2 half-life increased from 18 h to 31 h (**Fig. 2f**), indicating that TDP43 half-life in aggregates is different from that of diffuse TDP43, which would confound population-based estimates of protein half-life. We next removed from the analysis cells that died and therefore could have biased half-life calculations. When we did so, TDP43(WT)-Dendra2 half-life was significantly ($P = 0.0029$) longer (**Fig. 2f**). Thus, toxicity also affects measurements of protein half-life, artificially shortening values by eliminating cells before half-life can be measured. Alternatively, neurons with prolonged TDP43(WT)-Dendra2 half-life might live longer. In single-cell analyses, however, we detected no relationship between TDP43(WT)-Dendra2 half-life and survival (data not shown). Therefore, cell death most likely confounds population-based estimates of protein clearance by prematurely excluding cells from analysis. This is particularly evident with proteins, such as TDP43, whose levels are closely tied to survival.

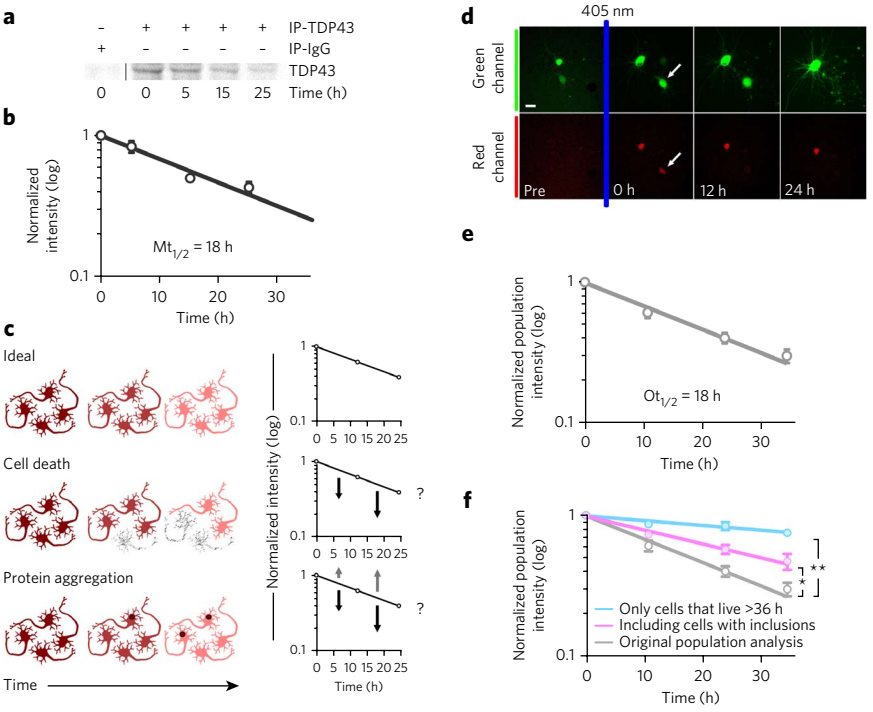

Figure 2 | Optical pulse-labeling of TDP43 in primary neurons. (**a**) Primary neurons were labeled with ^{35}S-labeled methionine, and TDP43 was immunoprecipitated using anti-TDP43 antibodies (IP-TDP43) or nonspecific IgG antibodies (IP-IgG). (**b**) Log-normal plot of normalized TDP43 levels. TDP43 half-life was determined by fitting a first-order exponential curve to the data ($R^2 = 0.8984$). Values were pooled from five independent experiments. (**c**) Potential confounders in half-life analyses. Top, total protein ideally decreases over time in a predictable manner (top right panel). Middle, toxicity reduces the amount of measured protein, potentially shortening the calculated half-life (middle right panel). Bottom, protein aggregation might also shorten half-life estimations if the protein cannot be immunoprecipitated (black arrows, bottom right panel) or lengthen it if the protein is more stable and successfully immunoprecipitated (gray arrows, bottom right panel). (**d**) OPL. Primary cortical neurons were transfected with EGFP and TDP43(WT)-Dendra2, photoconverted then imaged by AFM. Dead cells (arrows) were excluded at the time of death. Pre, before photoconversion. (**e**) The half-life of TDP43(WT)-Dendra2 was determined by fitting a first-order exponential curve to the data ($R^2 = 0.9558$). (**f**) Including cells with aggregates prolonged TDP43(WT)-Dendra2 half-life (pink line, $R^2 = 0.9003$; $^*P < 0.0001$, F 15.34, extra sum-of-squares F-test). Excluding cells that died over the 36-h experiment also prolonged half-life (cyan line, $R^2 = 0.7171$; $^{**}P < 0.0001$, extra sum-of-squares F-test). Error bars represent s.e.m. Values were pooled from eight wells per condition, with experiments performed in quadruplicate.

Pathogenic mutations enhance TDP43 turnover

We next used OPL to visualize neuronal TDP43 clearance. Neurons expressing TDP43(WT)-Dendra2 were photoconverted and tracked until an inclusion developed or cell death. For each neuron, we measured the red fluorescence of TDP43(WT)-Dendra2 immediately after photoconversion and used each cell as its own control to normalize subsequent measurements. Individual neurons exhibited marked variability in TDP43(WT)-Dendra2 half-life (**Fig. 3a**) that was independent of expression (**Supplementary Fig. 4c–e**). TDP43(WT)-Dendra2 half-life was significantly shorter as measured by single-cell analyses, in comparison to that measured by population-based methods (68 h versus 18 h; $P < 0.0001$, $F = 96.75$, extra sum-of-squares F-test). Therefore, in the absence of confounding from toxicity and aggregation, TDP43(WT)-Dendra2 half-life is substantially greater than previously estimated.

We next used OPL to determine whether pathogenic mutations affect TDP43 clearance. The median TDP43^{A315T}-Dendra2 half-life (50 h) was shorter than that of TDP43(WT)-Dendra2 (**Fig. 3a**), suggesting more rapid clearance of the mutant protein. We also analyzed single-cell half-life using a probability density function, confirming the effect of the A315T mutation on TDP43-Dendra2 half-life (**Fig. 3b–d**). We then used OPL to measure the half-life of TDP43-Dendra2 carrying a separate ALS-associated mutation, M337V (ref. 8) (**Supplementary Fig. 5a**), and we found that this mutation also reduced TDP43-Dendra2 half-life. Expression of mutant TDP43 might trigger global changes in protein catabolism, but we found no difference in the half-life of unrelated, Dendra2-fused proteins in neurons expressing WT or mutant TDP43 (data not shown). Therefore, our observations strongly suggest that *TARDBP* mutations associated with ALS stimulate TDP43 clearance.

Induction of autophagy increases TDP43 clearance

We chose to stimulate TDP43 clearance through autophagy because this pathway degrades long-lived cytoplasmic proteins and

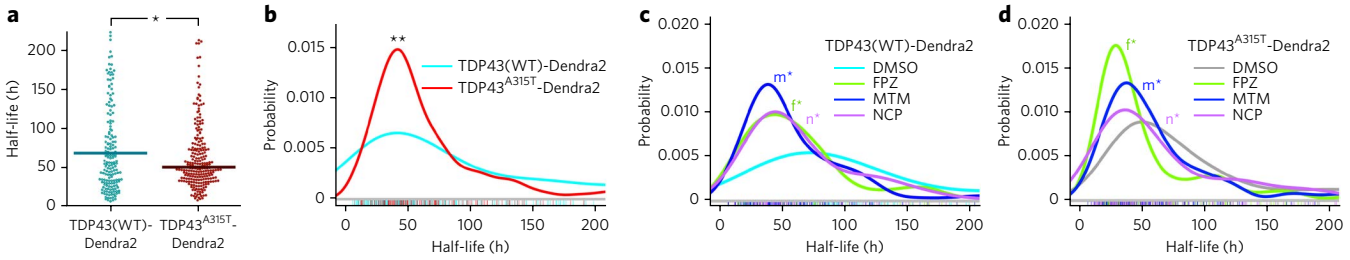

Figure 3 | OPL of TDP43. (**a**) Scatter plot depicting half-life measurements for individual cells expressing TDP43(WT)-Dendra2 (cyan, $n = 206$) and TDP43^{A315T}-Dendra2 (red, $n = 251$). *$P = 0.0029$, U = 11,797, Mann-Whitney test. (**b**) Probability density plot for single-cell half-life measurements, demonstrating a reduced half-life of TDP43^{A315T}-Dendra2 (red, $n = 251$), compared to TDP43(WT)-Dendra2 (cyan, $n = 206$; **$P = 0.0007$, two-sided Kolmogorov-Smirnov test). Values were pooled from eight wells per condition, with experiments performed in quadruplicate. (**c**,**d**) Probability density plots of single-cell half-life measurements for TDP43(WT)-Dendra2 (**c**) and TDP43^{A315T}-Dendra2 (**d**). At 0.5 μM, all three of the compounds significantly reduced TDP43(WT)-Dendra2 half-life compared to vehicle control (DMSO, $n = 110$; FPZ, $n = 96$, f* $P = 1 \times 10^{-4}$; MTM, $n = 129$, m* $P = 2 \times 10^{-7}$; NCP, $n = 111$, n* $P = 2 \times 10^{-5}$, two-sided Kolmogorov-Smirnov test). The compounds also reduced TDP43^{A315T}-Dendra2 half-life, in comparison to vehicle control (DMSO, $n = 120$; FPZ, $n = 155$, f* $P = 2 \times 10^{-9}$; MTM, $n = 152$, m* $P = 0.004$; NCP, $n = 111$, n* $P = 0.005$, two-sided Kolmogorov-Smirnov test). Colored hash marks represent values from individual neurons in **b**–**d**. Values were obtained from eight wells per condition, with experiments performed in triplicate.

organelles[28] and cytoplasmic accumulation of TDP43 is toxic[9]. Using a neuronal autophagy-inducing pharmacophore[22], we screened an *in silico* library of over 1 million compounds for more potent autophagy stimulators (Online Methods). The top two candidates from this screen, fluphenazine (FPZ, **1**) and methotrimeprazine (MTM, **2**), and the lead compound 10-(4′-(*N*-diethylamino)butyl)-2-chlorophenoxazine (NCP, **3**) were selected for study. We previously demonstrated that NCP effectively induces neuronal autophagy[22]. Here, all three compounds increased levels of LC3-II, the lipidated isoform of light chain 3 isoform I (LC3-I) that is incorporated into developing autophagosomes[29], and the LC3-II/LC3-I ratio in primary rodent cortical neurons (**Fig. 4a–c** and **Supplementary Fig. 6a**), confirming their efficacy in stimulating autophagy. All of the compounds also stimulated LC3-positive puncta formation and enhanced LC3-II/LC3-I ratios in the presence of NH_4Cl, an alkalinizing agent that prevents autophagosome maturation[29] (**Supplementary Fig. 6b–i**), verifying autophagy induction. We reliably detected such effects at 5 μM but not 0.5 μM, suggesting a dose-dependent response, limited assay sensitivity or both.

The limitations of these techniques for demonstrating autophagic induction are myriad[29]. Fundamentally, they depend on inferring autophagic flux from changes in levels of intermediates under specific conditions. To accurately measure flux, the rate of protein breakdown must be measured directly for an autophagy substrate. We therefore developed an *in situ* assay of autophagy flux by fusing LC3 to Dendra2, expressing LC3-Dendra2 in primary

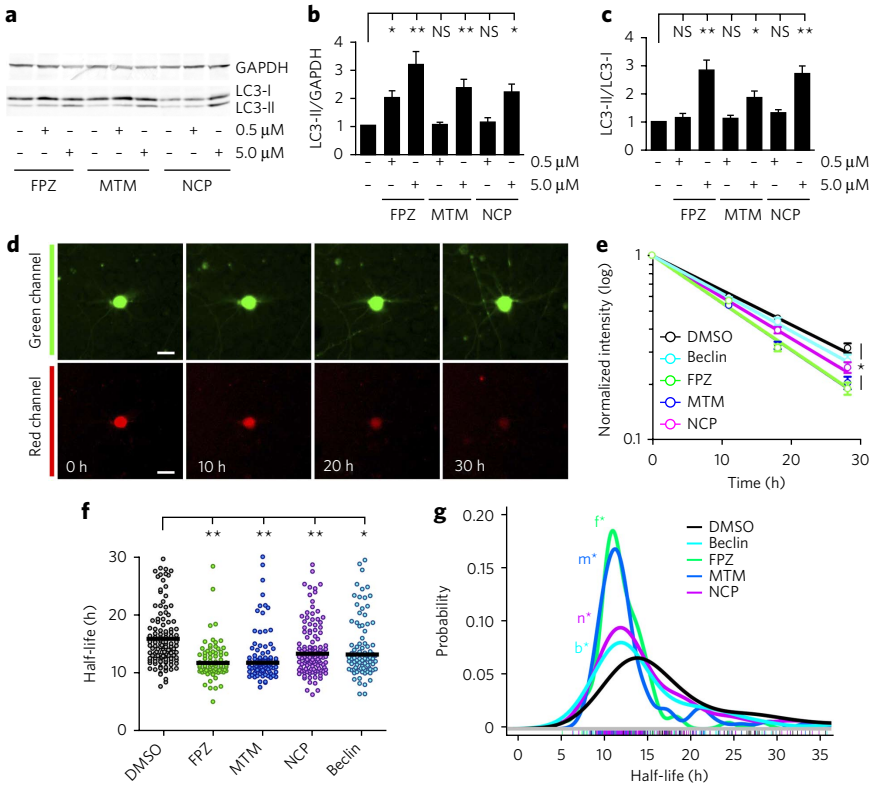

Figure 4 | Induction of autophagy by a family of small molecules. (**a**) Each of the compounds induced LC3-II in primary neurons, as determined by western blotting. At 5 μM but not 0.5 μM, the compounds significantly increased LC3-II/GAPDH (**b**) and LC3-II/LC3-I (**c**) ratios (nonsignificant (NS), $P > 0.05$; $0.05 < *P < 0.01$, $**P < 0.01$; $F = 13.74$ (in **b**) and 9.74 (in **c**), one-way ANOVA with Dunnett's post-test). Error bars represent s.e.m. Values were pooled from five independent experiments. (**d**) Optical pulse labeling of LC3-Dendra2 in rodent primary cortical neurons. Scale bars, 25 μm. (**e**) The change in red fluorescence intensity over time was used to calculate LC3-Dendra2 half-life, as in **Figure 2** (DMSO, $R^2 = 0.7333$; Beclin, $R^2 = 0.6968$, FPZ, $R^2 = 0.8752$; MTM, $R^2 = 0.8447$; NCP, $R^2 = 0.8357$; $*P < 0.0001$ for global trend, $F = 12.6$, extra sum-of-squares F-test). Error bars represent s.e.m. (**f**) The median single-cell half-life of LC3-Dendra2 was significantly reduced by beclin expression or treatment with 0.5 μM NCP, MTM or FPZ ($*P < 0.01$, $**P < 0.001$, Kruskal Wallis statistic = 52.56, Kruskal-Wallis with Dunn's test). (**g**) Probability density plot of LC3-Dendra2 half-life measurements from individual neurons treated with vehicle control (DMSO, $n = 140$), NCP ($n = 128$), MTM ($n = 91$), FPZ ($n = 77$) or those expressing beclin ($n = 101$). n*, $P = 6 \times 10^{-4}$; m*, $P = 1 \times 10^{-10}$; f*, $P = 5 \times 10^{-9}$; b*, $P = 2 \times 10^{-3}$; two-sided Kolmogorov-Smirnov test). Colored hash marks represent values from individual neurons. Values were pooled from eight wells per condition, with experiments performed in triplicate.

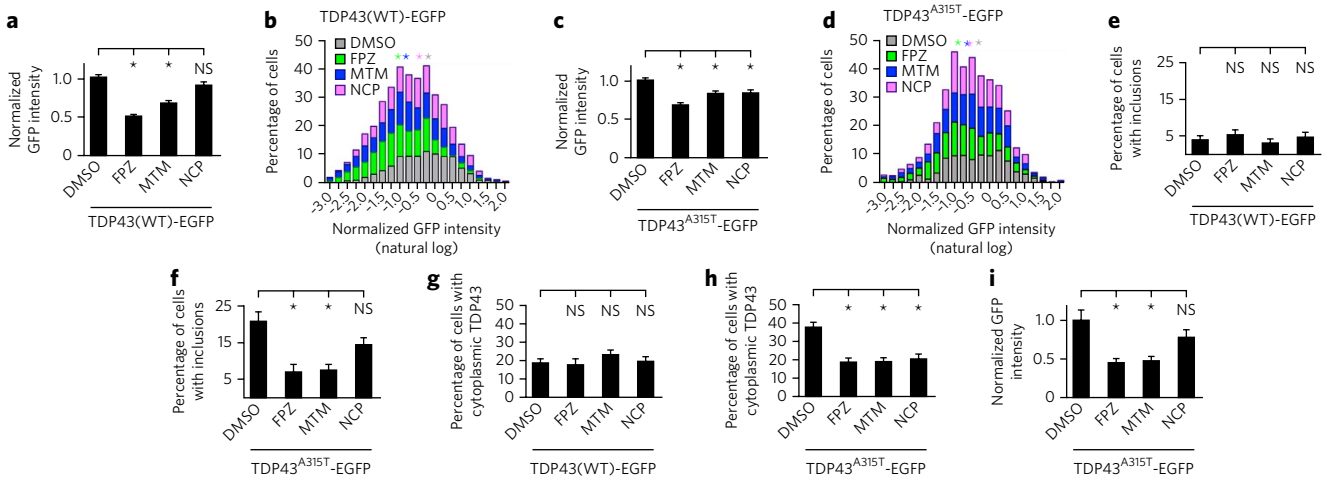

Figure 5 | Autophagy induction reduces TDP43 levels, aggregation and cytoplasmic mislocalization. (**a**) FPZ (n = 490) and MTM (n = 580) but not NCP (n = 523) lowered total TDP43(WT)-EGFP levels in comparison to vehicle (DMSO, n = 1,007). (**b**) Histogram of normalized, log-transformed TDP43(WT)-EGFP levels. (**c**) Each compound also reduced TDP43^{A315T}-EGFP levels (DMSO, n = 983; FPZ, n = 550; MTM, n = 542; NCP, n = 493). (**d**) Histogram of single-cell TDP43(A315T)-EGFP levels. Asterisks in **b** and **d** denote median values for cells exposed to vehicle (gray), FPZ (green), MTM (blue) or NCP (purple). For FPZ, MTM and NCP versus DMSO in **a** and **d**, $P < 1 \times 10^{-3}$ by two-sided Kolmogorov-Smirnov test. (**e**) No compound reduced TDP43(WT)-EGFP inclusions 48 h after transfection (DMSO, n = 360; FPZ, n = 194; MTM, n = 234; NCP, n = 203). (**f**) FPZ and MTM but not NCP reduced TDP43^{A315T}-EGFP inclusions at 48 h (DMSO, n = 327; FPZ, n = 226; MTM, n = 262; NCP, n = 253). (**g**) No compound affected TDP43(WT)-EGFP localization 24 h after transfection (DMSO, n = 256; FPZ, n = 212; MTM, n = 250; NCP, n = 241). (**h**,**i**) Each compound (**h**) prevented TDP43^{A315T}-EGFP cytoplasmic mislocalization (DMSO, n = 233; FPZ, n = 268; MTM, n = 263; NCP, n = 270) and reduced cytoplasmic TDP43(A315T)-EGFP levels (DMSO, n = 125; FPZ, n = 102; MTM, n = 121; NCP, n = 144. *P < 0.05; NS, P > 0.05) (**i**). For **a**, **c** and **e**–**i**, *P < 0.05; nonsignificant (NS), P > 0.05, one-way ANOVA with Dunnett's test. Error bars represent s.e.m. Values in **a**–**d** were pooled from 8–12 wells per condition from six experiments, values in **e**–**h** were pooled from eight wells per condition from three experiments, and values in **i** were pooled from five wells per condition from two experiments.

rodent cortical neurons (**Fig. 4d**) and measuring the turnover of LC3-Dendra2 through OPL. First, we used this assay to investigate autophagic flux in response to NCP, MTM and FPZ. As a positive control, we cotransfected neurons with beclin, an autophagy upregulator[30]. Beclin expression reduced the median LC3-Dendra2 half-life, as did treatment with NCP, MTM and FPZ (**Fig. 4e**,**f**). In single-cell analyses (**Fig. 4g**), we noted that 0.5 μM of each compound, which is one-tenth the dose required in conventional assays (**Fig. 4a**–**c**), effectively shortened LC3-Dendra2 half-life, suggesting that OPL is substantially more sensitive than traditional measures. To ensure that the compounds were stimulating autophagy and not acting through off-target pathways, we measured the effects of the compounds in cells depleted of the essential autophagy protein Atg7 (ref. 31) (**Supplementary Fig. 6j**). As expected, Atg7 knockdown prolonged LC3-Dendra2 half-life. No compound reduced LC3-Dendra2 half-life in Atg7-knockdown neurons, indicating that their effects on LC3-Dendra2 flux are mediated specifically through autophagy.

In population-based approaches (**Fig. 4e**,**f**), FPZ and MTM appeared to affect autophagic flux similarly. However, in single-cell analyses (**Fig. 4g**), subtle differences were evident: we noted a slightly higher 'peak' in FPZ-treated neurons and less of a 'shoulder' representing neurons with relatively long LC3-Dendra2 half-lives. These observations suggest that FPZ is a more potent autophagy inducer and illustrate the advantages of single-cell approaches over traditional methods for evaluating target efficacy.

We next asked whether the compounds enhance TDP43 clearance. Primary neurons expressing WT and mutant TDP43-Dendra2 were treated with vehicle (DMSO) or 0.5 μM of each compound, and half-life was determined through OPL. Probability density plots demonstrated effective reduction in TDP43-Dendra2 half-life with each compound (**Fig. 3c**,**d**). Thus, all three compounds augment WT and mutant TDP43-Dendra2 clearance in primary neurons by inducing autophagy.

Autophagy induction improves TDP43 metabolism

We wondered whether enhancing TDP43 turnover might directly affect TDP43 levels, subcellular localization and aggregation. To answer this question, we expressed WT or mutant TDP43-EGFP in primary neurons, treated the cultures with vehicle or 0.5 μM of each compound and imaged the neurons by AFM. Because TDP43 shuttles between the nucleus and cytoplasm[4], augmenting TDP43 turnover within the cytoplasm through autophagy should lower whole-cell TDP43 levels. FPZ and MTM but not NCP significantly ($P < 1 \times 10^{-3}$) decreased TDP43(WT)-EGFP levels (**Fig. 5a**) and shifted the distribution of expression to the left (**Fig. 5b**), consistent with their effects on protein half-life (**Fig. 3c**). All three also lowered whole-cell TDP43^{A315T}-EGFP levels (**Fig. 5c**) and left-shifted the TDP43^{A315T}-EGFP expression distribution (**Fig. 5d**). Very few neurons displayed TDP43(WT)-EGFP inclusions (**Fig. 5e** and **Supplementary Fig. 1**). However, almost 20% of neurons expressing TDP43^{A315T}-EGFP developed inclusions by 48 h (**Fig. 5f**), a figure reduced by FPZ and MTM but not NCP. FPZ and MTM were more effective than NCP in stimulating autophagy (**Fig. 4**), implying that the observed reductions in TDP43-EGFP levels and aggregation are proportional to autophagy induction.

In agreement with our prior observations[9], the A315T mutation increased the proportion of neurons with cytoplasmic TDP43-EGFP (**Fig. 5g**,**h**). We surmised that stimulating autophagy might also reduce cytoplasmic TDP43-EGFP mislocalization. Autophagy induction effectively reduced the proportion of neurons with cytoplasmic TDP43^{A315T}-EGFP without changing the localization of TDP43(WT)-EGFP. We also noted a reduction of cytoplasmic TDP43^{A315T}-EGFP levels with FPZ and MTM but not with NCP (**Fig. 5i**), mirroring the compounds' respective abilities to shorten TDP43^{A315T}-EGFP half-life (**Fig. 3d**). These data provide strong evidence that autophagic stimulation lowers WT and mutant TDP43 levels and reduces mutant TDP43 cytoplasmic mislocalization and aggregation.

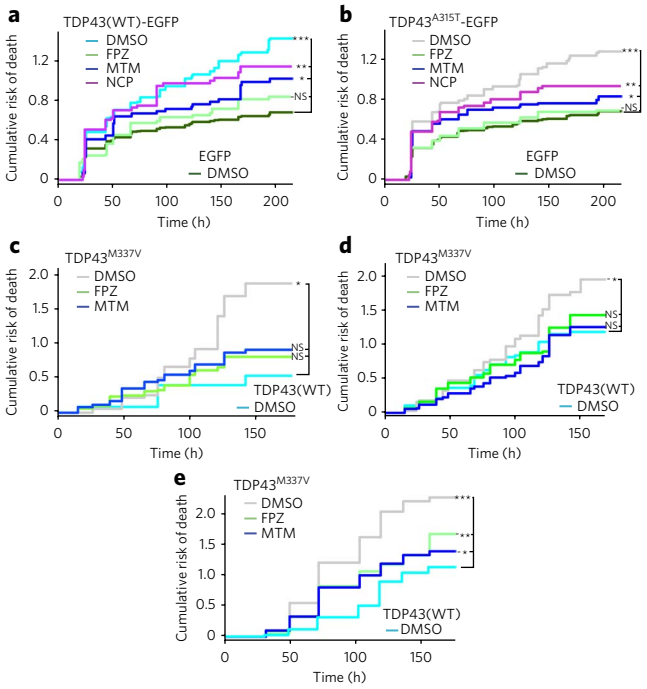

Figure 6 | Autophagic stimulation improves survival in neuronal and astrocyte models of ALS. (**a**,**b**) Primary neurons transfected with TDP43(WT)-EGFP (**a**) or TDP43^{A315T}-EGFP (**b**) were treated with autophagy inducers and survival determined by AFM. Data were obtained from eight wells per condition, with experiments performed in triplicate. **Supplementary Table 2** lists the number of neurons per condition, hazard ratios, 95% CI and *P* values, as determined by Cox hazards analysis. (**c**) Autophagic induction improved survival in TDP43^{M337V} HB9-positive human iPSC-derived MNs. (**d**) FPZ and MTM also reduced the risk of death in MAP2-positive human iPSC-derived MNs Values in **c** and **d** were pooled from 18 wells per condition, with experiments performed in triplicate. (**e**) Astrocytes differentiated from human iPSCs exhibit mutant TDP43-related toxicity that is mitigated by FPZ and MTM. Values were pooled from 18 wells per condition, performed in triplicate. **Supplementary Table 3** lists the number of human iPSC-derived neurons and astrocytes per condition, hazard ratios, 95% CI and *P* values, as determined by Cox hazards analysis.

Autophagy induction prevents TDP43-mediated cell death

If TDP43 levels and mislocalization are proximal drivers of toxicity and autophagy induction affects both factors, autophagy induction should improve survival. To test this, we expressed WT and mutant TDP43-EGFP at levels two- to threefold higher than endogenous levels in primary neurons and imaged cells by AFM (**Fig. 6a**,**b**). At 0.5 μM, FPZ and MTM but not NCP improved survival (**Supplementary Table 2**). Neither FPZ nor MTM affected the survival of control neurons expressing EGFP alone (**Supplementary Fig. 2b**–**e**). FPZ also improved survival in neurons expressing a different TDP43 mutant, TDP43^{M337V}-EGFP (**Supplementary Fig. 5b**). We attribute the ineffectiveness of NCP to off-target, compound-specific toxicity that most likely counteracts any protective effects mediated by autophagy induction (**Supplementary Fig. 2c**).

We next asked whether the benefits of autophagy induction might be explained through its effects on TDP43 levels or localization. FPZ lowered TDP43(WT)-EGFP levels by 50% and TDP43^{A315T}-EGFP levels by 32% (**Fig. 5a**–**d**). According to dose-response plots (**Fig. 1f**,**g**), a 50% reduction in WT TDP43 levels should lower the experimental HR from 1.9 to 1.28, for a predicted HR of 0.67. The actual HR for the FPZ-treated group was 0.60 (**Fig. 6a**), suggesting that the beneficial effect of autophagic induction can be largely explained by proportional reduction in WT TDP43 levels. For mutant TDP43, a 32% decrease in levels should lower the experimental HR from 1.8 to 1.31, resulting in a predicted HR of 0.73. As the actual HR (0.60) for neurons treated with FPZ is better than predicted (0.73; **Fig. 6b**), stimulating autophagy most likely has additional beneficial effects; for instance, autophagy induction also prevents mutant TDP43 mislocalization and reduces cytoplasmic TDP43 levels (**Fig. 5h**,**i**), which we reported to be neurotoxic[9].

For autophagy inducers to be valid ALS therapies, they must mitigate neurodegeneration in human neurons and astrocytes. We therefore tested the two most potent autophagy inducers, MTM and FPZ, in human stem cell–based ALS models. In prior studies, motor neurons (MNs) derived from human induced pluripotent stem cells (iPSCs) carrying a pathogenic *TARDBP* mutation (M337V) exhibited a greater risk of death than WT neurons[32]. To determine whether stimulating autophagy might prevent mutant TDP43-mediated toxicity in human MNs, we differentiated MNs from WT TDP43 and TDP43^{M337V} iPSCs[32] and introduced a MN-specific survival marker driven by the HB9 promoter[33]. Cultures were treated with vehicle or 0.5 μM of each compound, and neuronal survival was determined by AFM (**Fig. 6c**). As expected, TDP43^{M337V} MNs demonstrated an elevated risk of death compared to WT TDP43 MNs (**Supplementary Table 3**). MTM and FPZ reduced the risk of death for TDP43^{M337V} MNs without affecting the survival of WT TDP43 MNs (**Supplementary Fig. 7a**). Although ALS typically begins with MN dysfunction and loss, it evolves into a multisystem disorder affecting several different neuronal subtypes[34]. Therefore, we also evaluated the compounds in iPSC-derived neurons expressing a pan-neuronal MAP2 survival marker[35] (**Fig. 6d**). As with HB9-positive MNs, MTM and FPZ reduced risk of death in TDP43^{M337V} MAP2-positive neurons without causing toxicity in WT iPSC-derived neurons (**Supplementary Fig. 7b**).

Astrocytes are integrally involved in ALS onset and progression[36]. We reported an increased risk of death in human astrocytes harboring TDP43^{M337V} (ref. 37), indicative of intrinsic toxicity related to pathogenic *TARDBP* mutations. To determine whether autophagy induction is beneficial in human TDP43^{M337V} astrocytes, we differentiated WT and mutant iPSCs into astrocytes, transfected them with mApple and determined the time of death by AFM (**Fig. 6e** and **Supplementary Table 3**). TDP43^{M337V} astrocytes had an elevated risk of death that was effectively diminished by 0.5 μM FPZ and MTM. Neither compound affected the survival of WT TDP43 astrocytes (**Supplementary Fig. 7c**). Inducing autophagy is thus an effective and safe strategy for reducing mutant TDP43-associated toxicity in human neurons and astrocytes.

DISCUSSION

Here, we measured protein turnover *in situ* by OPL and showed that, in comparison to conventional methods, OPL is particularly advantageous for investigations of neurodegenerative diseases, where the implicated proteins are toxic and prone to misfolding. We also established a new autophagic flux assay that can be applied on a single-cell basis, and through an *in silico* screen we identified compounds that effectively stimulate autophagy in neurons, enhance TDP43 clearance and reduce its mislocalization. Finally, and perhaps most notably, we demonstrated that autophagy induction improves survival in human iPSC-derived neurons and astrocytes from patients with familial ALS, the most genetically precise disease models currently available.

Fueled by autophagy's broad therapeutic potential, interest in this pathway has grown exponentially. Still, the lack of high-throughput screening assays limits the discovery and development of autophagy inducers as therapies[29]. Here, we designed and validated a live-cell autophagic flux assay that is uniquely suited to high-throughput and high-content screening: it is robust, quantitative and adaptable

to any cell type. LC3 clearance in this assay was tightly correlated with autophagic flux, and although definitive proof of this will require equally sensitive measures of autophagic maturation, the assay represents a major advance over prior screening methods, and we expect it to facilitate the identification of new autophagy-inducing agents.

Regardless of the model system, the most important factor in determining neuronal survival is the steady-state level of TDP43: elevated levels are invariably associated with more aggressive neurodegeneration[10,11]. In sALS, WT TDP43 accumulates within the neuronal cytoplasm[2], indicating that protein levels and localization may be primary drivers of neurodegeneration not only in fALS, when they are precipitated by *TARDBP* mutations, but also in sALS. Our data show that both WT and mutant TDP43 levels are linearly related to toxicity, with nearly identical slopes, suggesting that ALS-associated *TARDBP* mutations might cause toxicity by increasing TDP43 levels[32,38] or mislocalization[9,37]. Strategies that reduce TDP43 levels and mislocalization, including autophagy induction as shown here, may therefore be effective in both sALS and fALS.

We sought to improve neuronal survival by enhancing TDP43 clearance via small-molecule autophagy inducers. With these compounds, we tested the utility of autophagy induction for desired on-target effects (e.g., TDP43 clearance) and for efficacy against disease-related phenotypes (e.g., survival). The compounds represent well-validated tools for inducing autophagy in neurons, but they and their derivatives must be evaluated *in vivo* to assess for therapeutic effectiveness or unanticipated toxicities. Still, phenothiazine derivatives, including FPZ, have been used for decades to treat patients with psychoses. These compounds appear to be neuroprotective[39], and one phenothiazine derivative, pimozide[40], slowed disease progression in ALS patients. Because of its structural similarity to NCP, we tested pimozide in our initial screen[22] and found that it does in fact stimulate autophagy, providing indirect support for the beneficial effects of autophagy induction in ALS.

We modeled disease mechanisms over a short time by capitalizing upon a marked and conserved pathologic signature among neurodegenerative diseases: the accumulation of misfolded proteins, such as TDP43. Overexpressing TDP43 in primary neurons reproduces key hallmarks of ALS pathology, including neurodegeneration accompanied by TDP43 accumulation and mislocalization[9]. Coping responses in acute overexpression models may be different from those occurring in ALS patients, representing a potential caveat of the current system. Still, human iPSC-derived neurons and astrocytes carrying ALS-associated mutations in *TARDBP* also accumulate mutant TDP43 protein[32,37], lending additional support to the notion that excess TDP43 is central to disease pathogenesis. Autophagy induction effectively improved survival in rodent neurons and in human iPSC-derived neurons and astrocytes, supporting the validity of the rodent model system used here and, more importantly, showing that enhancing TDP43 clearance is a reasonable neuroprotective strategy for humans with disease.

In a prior study[20], rapamycin exhibited neuroprotective effects in TDP43 transgenic animals, but there was little evidence that the benefit was tied to autophagy induction. Rapamycin and other mTOR inhibitors exert multiple effects independent of autophagy[23], including some (for example, inhibition of protein synthesis[41]) that account for their benefits in another disease model[42]. The concentrations typically used to mitigate disease are much higher than the half-maximum effective concentration associated with mTOR inhibition, raising serious concerns about their mechanisms of action. In contrast, we identified compounds that effectively stimulate neuronal autophagy and enhance TDP43 turnover. This, in turn, reduced the amount of TDP43, explaining much of the survival benefit observed in primary neurons and human iPSC-derived neurons and astrocytes.

Increasing evidence suggests that non-neuronal phenomena contribute to ALS pathogenesis[36]. For instance, mutant TDP43 exhibits intrinsic toxicity in human astrocytes, and these cells enhance the survival of iPSC-derived neurons[37]. Previous investigations of autophagy stimulation in ALS[20] failed to determine whether neuronal or glial induction was responsible for the observed benefit, an essential question relating to the drugs' targets and mechanism of action. We measured autophagic activation at the single-cell level, within living neurons, leaving no doubt as to the targeted cell type.

Given the relatively rapid clearance of mutant TDP43, we wondered why it preferentially accumulates in fALS. In previous work[9], we showed that $TDP43^{A315T}$ forms detergent-resistant inclusions more readily than WT TDP43. If mutant TDP43 misfolding and deposition outpace degradation, kinetics will favor the formation of inclusions, despite mutant TDP43's relatively short half-life. According to this model, stabilization of mutant TDP43 through aggregation can be prevented by blocking TDP43 misfolding or enhancing its degradation before inclusions form. Autophagy inducers most likely accomplish the latter, effectively augmenting mutant TDP43 clearance and inhibiting the formation of visible TDP43 inclusions. Stimulating autophagy may also improve proteostasis more generally, which could also indirectly improve protein misfolding.

One of the biggest obstacles to therapy development is the unreliable translation from preclinical disease models to humans[43]. iPSC-derived neurons and astrocytes have the potential to transform therapeutics development for ALS and other disorders[44]. Here, we observed neuroprotection in iPSC-based ALS models, without the use of artificial stressors to elicit phenotypes[38]. Astrocytes prevent[37,45] or stimulate[46] neuronal loss under different circumstances and are directly affected by disease-associated mutations[37]. Our results, demonstrating efficacy of small-molecule autophagy inducers in human iPSC-derived neurons and astrocytes, suggests that a common therapeutic strategy might work in more than one cell type.

In prior work, we showed that visible TDP43 inclusions do not affect neuronal survival[9], and multiple *in vivo* studies have confirmed that TDP43 inclusions are not required for neurotoxicity[10,11]. Strong precedence exists for the idea that protein inclusions themselves are not necessarily pathogenic[25,47,48]. Thus, although autophagy induction reduced visible inclusions in $TDP43^{A315T}$-expressing neurons, we do not believe this directly affected survival. Instead, the observed reduction in inclusions most likely followed the drop in TDP43 levels or cytoplasmic localization, as inclusions develop preferentially in cells with high TDP43 levels[9], and they are predominantly cytoplasmic.

Neuronal inclusions rich in misfolded proteins are characteristic of Huntington's disease and ALS, consistent with underlying protein dyshomeostasis in both disorders. Our current and previous[49] results suggest that neurons cope with aggregation-prone proteins by targeting them for accelerated clearance. Instead of a nonspecific reaction to overexpressed proteins, this may represent a conserved coping response directed against toxic, misfolded proteins. When the cell's ability to degrade these proteins is insufficient, the proteins accumulate and cause toxicity. Thus, enhancing protein clearance should prevent accumulation and improve survival. We tested this by inducing autophagy and found that stimulating TDP43 clearance via autophagy reduced TDP43 levels and diminished risk of death. These data show that protein dyshomeostasis is a common thread in neurodegenerative diseases and offer the exciting hope that therapies targeting this thread might have broad therapeutic potential.

Received 29 October 2013; accepted 19 May 2014;
published online 29 June 2014

METHODS

Methods and any associated references are available in the online version of the paper.

References

1. Robberecht, W. & Philips, T. The changing scene of amyotrophic lateral sclerosis. *Nat. Rev. Neurosci.* **14**, 248–264 (2013).
2. Neumann, M. Molecular neuropathology of TDP-43 proteinopathies. *Int. J. Mol. Sci.* **10**, 232–246 (2009).
3. van Blitterswijk, M. & Landers, J.E. RNA processing pathways in amyotrophic lateral sclerosis. *Neurogenetics* doi:10.1007/s10048-010-0239-4 (2010).
4. Ayala, Y.M. *et al.* Structural determinants of the cellular localization and shuttling of TDP-43. *J. Cell Sci.* **121**, 3778–3785 (2008).
5. Moisse, K. *et al.* Cytosolic TDP-43 expression following axotomy is associated with caspase 3 activation in *NFL*$^{-/-}$ mice: support for a role for TDP-43 in the physiological response to neuronal injury. *Brain Res.* **1296**, 176–186 (2009).
6. Dewey, C.M. *et al.* TDP-43 is directed to stress granules by sorbitol, a novel physiological osmotic and oxidative stressor. *Mol. Cell. Biol.* **31**, 1098–1108 (2011).
7. Davidson, Y.S. *et al.* TDP-43 pathological changes in early onset familial and sporadic Alzheimer's disease, late onset Alzheimer's disease and Down's Syndrome: association with age, hippocampal sclerosis and clinical phenotype. *Acta Neuropathol.* **122**, 703–713 (2011).
8. Barmada, S.J. & Finkbeiner, S. Pathogenic TARDBP mutations in amyotrophic lateral sclerosis and frontotemporal dementia: disease-associated pathways. *Rev. Neurosci.* **21**, 251–272 (2010).
9. Barmada, S.J. *et al.* Cytoplasmic mislocalization of TDP-43 is toxic to neurons and enhanced by a mutation associated with familial amyotrophic lateral sclerosis. *J. Neurosci.* **30**, 639–649 (2010).
10. Tsao, W. *et al.* Rodent models of TDP-43: recent advances. *Brain Res.* **1462**, 26–39 (2012).
11. Roberson, E.D. Mouse models of frontotemporal dementia. *Ann. Neurol.* **72**, 837–849 (2012).
12. Ling, S.-C. *et al.* ALS-associated mutations in TDP-43 increase its stability and promote TDP-43 complexes with FUS/TLS. *Proc. Natl. Acad. Sci. USA* **107**, 13318–13323 (2010).
13. Watanabe, S., Kaneko, K. & Yamanaka, K. Accelerated disease onset with stabilized familial Amyotrophic Lateral Sclerosis (ALS)-linked TDP-43 mutations. *J. Biol. Chem.* **288**, 3641–3654 (2013).
14. Roscic, A., Baldo, B., Crochemore, C., Marcellin, D. & Paganetti, P. Induction of autophagy with catalytic mTOR inhibitors reduces huntingtin aggregates in a neuronal cell model. *J. Neurochem.* **119**, 398–407 (2011).
15. Prakash, A. & Levy, D.E. Regulation of IRF7 through cell type–specific protein stability. *Biochem. Biophys. Res. Commun.* **342**, 50–56 (2006).
16. Wang, X. *et al.* Degradation of TDP-43 and its pathogenic form by autophagy and the ubiquitin-proteasome system. *Neurosci. Lett.* **469**, 112–116 (2010).
17. Urushitani, M., Sato, T., Bamba, H., Hisa, Y. & Tooyama, I. Synergistic effect between proteasome and autophagosome in the clearance of polyubiquitinated TDP-43. *J. Neurosci. Res.* **88**, 784–797 (2010).
18. Zhang, X. *et al.* Rapamycin treatment augments motor neuron degeneration in SOD1^{G93A} mouse model of amyotrophic lateral sclerosis. *Autophagy* **7**, 412–425 (2011).
19. Hetz, C. *et al.* XBP-1 deficiency in the nervous system protects against amyotrophic lateral sclerosis by increasing autophagy. *Genes Dev.* **23**, 2294–2306 (2009).
20. Wang, I.-F. *et al.* Autophagy activators rescue and alleviate pathogenesis of a mouse model with proteinopathies of the TAR DNA-binding protein 43. *Proc. Natl. Acad. Sci. USA* **109**, 15024–15029 (2012).
21. Fox, J.H. *et al.* The mTOR kinase inhibitor Everolimus decreases S6 kinase phosphorylation but fails to reduce mutant huntingtin levels in brain and is not neuroprotective in the R6/2 mouse model of Huntington's disease. *Mol. Neurodegener.* **5**, 26 (2010).
22. Tsvetkov, A.S. *et al.* A small-molecule scaffold induces autophagy in primary neurons and protects against toxicity in a Huntington disease model. *Proc. Natl. Acad. Sci. USA* **107**, 16982–16987 (2010).
23. Laplante, M. & Sabatini, D.M. mTOR signaling in growth control and disease. *Cell* **149**, 274–293 (2012).
24. Gitcho, M.A. *et al.* TDP-43 A315T mutation in familial motor neuron disease. *Ann. Neurol.* **63**, 535–538 (2008).
25. Arrasate, M., Mitra, S., Schweitzer, E.S., Segal, M.R. & Finkbeiner, S. Inclusion body formation reduces levels of mutant huntingtin and the risk of neuronal death. *Nature* **431**, 805–810 (2004).
26. Xu, Y.-F. *et al.* The pathological phenotypes of human TDP-43 transgenic mouse models are independent of downregulation of mouse Tdp-43. *PLoS ONE* **8**, e69864 (2013).
27. Chudakov, D.M., Lukyanov, S. & Lukyanov, K.A. Tracking intracellular protein movements using photoswitchable fluorescent proteins PS-CFP2 and Dendra2. *Nat. Protoc.* **2**, 2024–2032 (2007).
28. Wong, E. & Cuervo, A.M. Integration of clearance mechanisms: the proteasome and autophagy. *Cold Spring Harb. Perspect. Biol.* **2**, a006734 (2010).
29. Klionsky, D.J. *et al.* Guidelines for the use and interpretation of assays for monitoring autophagy in higher eukaryotes. *Autophagy* **4**, 151–175 (2008).
30. Wang, J. Beclin 1 bridges autophagy, apoptosis and differentiation. *Autophagy* **4**, 947–948 (2008).
31. Kim, J., Dalton, V.M., Eggerton, K.P., Scott, S.V. & Klionsky, D.J. Apg7p/Cvt2p is required for the cytoplasm-to-vacuole targeting, macroautophagy, and peroxisome degradation pathways. *Mol. Biol. Cell* **10**, 1337–1351 (1999).
32. Bilican, B. *et al.* Mutant induced pluripotent stem cell lines recapitulate aspects of TDP-43 proteinopathies and reveal cell-specific vulnerability. *Proc. Natl. Acad. Sci. USA* **109**, 5803–5808 (2012).
33. Singh Roy, N. *et al.* Enhancer-specified GFP-based FACS purification of human spinal motor neurons from embryonic stem cells. *Exp. Neurol.* **196**, 224–234 (2005).
34. Geser, F. *et al.* Clinical and pathological continuum of multisystem TDP-43 proteinopathies. *Arch. Neurol.* **66**, 180–189 (2009).
35. Kosik, K.S. & Finch, E.A. MAP2 and tau segregate into dendritic and axonal domains after the elaboration of morphologically distinct neurites: an immunocytochemical study of cultured rat cerebrum. *J. Neurosci.* **7**, 3142–3153 (1987).
36. Boillée, S., Vande Velde, C. & Cleveland, D.W. ALS: a disease of motor neurons and their nonneuronal neighbors. *Neuron* **52**, 39–59 (2006).
37. Serio, A. *et al.* Astrocyte pathology and the absence of non-cell autonomy in an induced pluripotent stem cell model of TDP-43 proteinopathy. *Proc. Natl. Acad. Sci. USA* doi:10.1073/pnas.1300398110 (2013).
38. Egawa, N. *et al.* Drug screening for ALS using patient-specific induced pluripotent stem cells. *Sci. Transl. Med.* **5**, 188lr2 (2012).
39. Stavrovskaya, I.G. Clinically approved heterocyclics act on a mitochondrial target and reduce stroke-induced pathology. *J. Exp. Med.* **200**, 211–222 (2004).
40. Szczudlik, A., Tomik, B., Słowik, A. & Kasprzyk, K. Assessment of the efficacy of treatment with pimozide in patients with amyotrophic lateral sclerosis. Introductory notes. *Neurol. Neurochir. Pol.* **32**, 821–829 (1998).
41. Krauss, S. *et al.* Translation of HTT mRNA with expanded CAG repeats is regulated by the MID1–PP2A protein complex. *Nat. Commun.* **4**, 1511 (2013).
42. Miller, J. *et al.* Quantitative relationships between Huntingtin levels, polyglutamine length, inclusion body formation, and neuronal death provide novel insight into huntington's disease molecular pathogenesis. *J. Neurosci.* **30**, 10541–10550 (2010).
43. Finkbeiner, S. Bridging the Valley of Death of therapeutics for neurodegeneration. *Nat. Med.* **16**, 1227–1232 (2010).
44. Dolmetsch, R. & Geschwind, D.H. The Human brain in a dish: the promise of iPSC-derived neurons. *Cell* **145**, 831–834 (2011).
45. Jacquier, A., Bellouze, S., Blanchard, S., Bohl, D. & Haase, G. Astrocytic protection of spinal motor neurons but not cortical neurons against loss of Als2/alsin function. *Hum. Mol. Genet.* **18**, 2127–2139 (2009).
46. Haidet-Phillips, A.M. *et al.* Astrocytes from familial and sporadic ALS patients are toxic to motor neurons. *Nat. Biotechnol.* **29**, 824–828 (2011).
47. Ko, L.-W., Ko, H.-H.C., Lin, W.-L., Kulathingal, J.G. & Yen, S.-H.C. Aggregates assembled from overexpression of wild-type α-synuclein are not toxic to human neuronal cells. *J. Neuropathol. Exp. Neurol.* **67**, 1084–1096 (2008).
48. Mucke, L. *et al.* High-level neuronal expression of aβ 1–42 in wild-type human amyloid protein precursor transgenic mice: synaptotoxicity without plaque formation. *J. Neurosci.* **20**, 4050–4058 (2000).
49. Tsvetkov, A.S. *et al.* Proteostasis of polyglutamine varies among neurons and predicts neurodegeneration. *Nat. Chem. Biol.* **9**, 586–592 (2013).

Acknowledgments

We would like to thank B. Miller, B. Seeley, C. Lomen-Hoerth and the members of the Finkbeiner lab for their generous support and advice. H. Zahed and J. Margulis deserve special acknowledgment for their assistance. We thank G. Howard for editorial assistance and K. Nelson for administrative assistance. We also thank G. Yu and J. Herz (University of Texas, Southwestern) for anti-TDP43 antibodies. This work was supported by National Institutes of Neurological Disorders and Stroke grants K08 NS072233 (to S.J.B.), 3R01 NS039074, R01 NS083390, R43 NS081844 and U24 NS078370 (to S.F.); the ALS Association (S.F.); the Robert Packard Center for ALS Research and the William H. Adams Foundation (S.F.); and Target ALS (S.F.). Additional support was

provided by the Roddenberry Stem Cell Program (to S.F.), the Taube-Koret Center for Neurodegenerative Disease (S.F.), the Hellman Family Foundation Alzheimer's Disease Research Program (S.F.), the Protein Folding Diseases Initiative at the University of Michigan (S.J.B.) and the California Institute of Regenerative Medicine TR4-06693 (S.F.) and U01 MH1050135 (S.F.). The animal care facility was partly supported by an US National Institutes of Health Extramural Research Facilities Improvement Program Project (C06 RR018928).

Author contributions

S.J.B., A.S., A.A., A.T., S.C. and S.F. designed the study. S.J.B., A.A., X.L. and A.S. cultured cells, performed microscopy and conducted survival analyses. A.T., B.B., C.S. and S.C. provided compounds and iPSCs. M.P. performed *in silico* drug screening. D.P., D.M.A. and A.D. wrote original scripts for AFM. S.J.B. and A.A. analyzed data, constructed vectors, performed MPC and OPL and transfected neurons. S.B. and S.F. wrote and edited the manuscript.

Competing financial interests

The authors declare no competing financial interests.

Additional information

Supplementary information and chemical compound information is available in the online version of the paper. Reprints and permissions information is available online at http://www.nature.com/reprints/index.html. Correspondence and requests for materials should be addressed to S.F.

ONLINE METHODS

Ethics statement. Rat (*Rattus norvegicus*) colonies were maintained in accordance with the University of California–San Francisco, 'Assurance of Compliance with PHS Policy on Humane Care and Use of Laboratory Animals by Awardee Institutions' number A3400-01. The animal care facility at The J. David Gladstone Institutes is fully approved and under the supervision of full-time veterinarians. There were no manipulations that might have produced discomfort, distress, pain or injury. The animals were killed using CO_2, resulting in rapid and painless death, consistent with the recommendations of the Panel on Euthanasia of the American Veterinary Medical Association.

Plasmids. Human TDP43 fused at its C terminus to EGFP (TDP43-EGFP) was amplified from pcDNA-TDP43-EGFP[9] by PCR using the following primers: 5′-ATA TAT AAG CTT CCA TGT CTG AAT ATA TTC GGG TAA CCGA-3′ and 5′-ATA TAT GGT ACC GGA GAT CTC TTG TAC AGC TCG TCC ATGC-3′. Using KpnI and HindIII, the insert was then cloned into pGW1-CMV. Dendra2 was cloned into pGW1-CMV from pDendra2-N (Evrogen) using HindIII and MfeI. To create pGW1-TDP43-Dendra2, TDP43 was amplified by PCR using the following primers: 5′-TAT ATA AAG CTT CCA TGT CTG AAT ATA TTC GGG TAA CCGA-3′ and 5′- ATA TAT GGT ACC CCT CCC CAG CCA GAA GAC TTA GAA TCC-3′. The PCR product was digested with KpnI and HindIII and then inserted into pGW1-Dendra2 that had been cut with the same enzymes. The A315T mutation was established by site-directed mutagenesis using the following primers: 5′-GTG GTG GGA TGA ACT TTG GTA CGT TCA GCA TTA ATC CAG CC-3′ and 5′-GGC TGG ATT AAT GCT GAA CGT ACC AAA GTT CAT CCC ACC AC-3′. The M337V mutation was also created by site-directed mutagenesis using the following primers: 5′-GCA GTT GGG GTA TGG TGG GCA TGT TAG CC-3′ and 5′-GGC TAA CAT GCC CAC CAT ACC CCA ACT GC-3′. mApple was amplified by PCR from pmApple-C1 by the following primers: 5′-ATA TAA GCT TCG CCA CCA TGG TGA GCAA-3′ and 5′-ATA TGA ATT CTT ATC TAG ATC CGG TGG ATC CCG-3′. The insert was then ligated into pGW1-CMV after digestion with HindIII and EcoRI, creating pGW1-mApple. pGW1-EGFP and pGW1-Dendra2-LC3 were created as described[25,49]. To make the MAP2:mApple survival marker used in longitudinal microscopy of human iPSC-derived neurons, the human MAP2 promoter (Systems Biosciences) was cloned into pGW1-mApple using BamHI and XhoI. The HB9::GFP survival marker was generated as described[33]. Sequence information for all of the plasmids used is available at http://gind-db.ucsf.edu:8000/cgi-bin/Plasmid/main_menu2.cgi.

Cell culture and transfection. Cortical neurons were dissected from embryonic day 20–21 rat pups and cultured at 0.6×10^6 cells/ml for 4 d *in vitro*, as described[50]. Euthanasia for these experiments is entirely consistent with the recommendations of the Guidelines on Euthanasia of the American Veterinary Medical Association. Transfection of primary neurons was accomplished using Lipofectamine 2000 (Invitrogen). All of the transfections involved 0.2 µg DNA (total) and 0.5 µl Lipofectamine 2000 per well, unless otherwise noted. Cells were incubated with Lipofectamine–DNA complexes for no more than 20 min at 37 °C before rinsing. The remainder of the transfection protocol was per the manufacturer's suggestions. For cotransfections, plasmids were kept at a 1:1 molar ratio, unless otherwise noted in the text. For live-cell nuclear staining, neurons were incubated in PBS supplemented with calcium, magnesium and Hoechst dye (Life Technologies, H3569; 10 µM final concentration) for 10 min at 37 °C and were then transferred back to serum-free medium for imaging.

MPC. Primary rodent cortical neurons were isolated from embryonic day 21 rat pups as described above and cultured in six-well plates at a density of 0.6×10^6 cells/ml. On *in vitro* day 4, cultures were rinsed twice with methionine- and cysteine-free DME (Invitrogen) and then placed in the same medium for 1 h at 37 °C. Proteins were labeled by adding ^{35}S-labeled methionine and cysteine (EasyTag Express, PerkinElmer; final concentration 0.3 mCi/ml) and incubating for 4 h at 37 °C. Afterwards, neurons were rinsed twice with methionine- and cysteine-free DME and then cultured in Neurobasal medium supplemented with 2% B27, 1% GlutaMAX and 1% penicillin-streptomycin (all from Invitrogen). For collection, neurons were rinsed twice with ice-cold PBS then lysed in ice-cold RIPA (0.5% deoxycholate, 1% Triton X-100) supplemented with MiniProtean protease inhibitors (Roche). Samples were kept on ice for 5 min and then centrifuged at 1,000g for 5 min at room temperature. Supernatants were stored at −80 °C until all samples were collected. TDP43 was immunoprecipitated using rabbit polyclonal anti-TDP43 antibodies (G. Yu and J. Herz, University of Texas, Southwestern; ThermoScientific, PA5-17011, dilution 1:100) for 1 h at room temperature. As a control, nonspecific rabbit anti-IgG antibodies (Santa Cruz, sc-2027) were added at a similar concentration. Antibody–protein complexes were isolated using protein-A agarose beads (Invitrogen) diluted 1:20, by rotating for 30 min at room temperature. The complexes were rinsed twice with RIPA and twice more with PBS, before elution by boiling in Laemmli sample buffer. Proteins were separated by SDS-PAGE, and gels were fixed in 10% glacial acetic acid, 20% methanol, 3% glycerol (v/v/v) in water for 1 h at room temperature. Gels were then dried by heating to 80 °C for 2 h, under vacuum for 3 h. Dried gels were exposed to film (Kodak BioMax MR) with an intensifying screen overnight at −80 °C before developing. The amount of immunoprecipitated TDP43 at each time point was determined by densitometry of scanned films using ImageJ software and normalized to the amount of TDP43 at the initial time point.

Western blotting. Primary rodent cortical neurons were isolated and cultured from embryonic day 21 rat pups as described above in six-well plates at a density of 0.6×10^6 cells/ml. On *in vitro* day 5, cultures were treated with vehicle control (DMSO), 0.5 µM or 5 µM of compound for 24 h. Cells were rinsed twice in ice-cold PBS and lysed in RIPA (0.5% deoxycholate, 1% Triton X-100) supplemented with MiniProtean protease inhibitors (Roche). Lysates were separated by SDS-PAGE, and proteins were detected via western blotting. Primary antibodies included rabbit polyclonal anti-LC3 antibodies raised against a polypeptide modeled after the N terminus of LC3 (EKTFKQRRSFEQRVEDVR), diluted 1:1,000 in 1% nonfat dry milk (Bio-Rad) in TBS-T (Tris-buffered saline with 0.1% Tween-20) and mouse monoclonal anti-GAPDH antibodies (AbCam, 6C5) diluted 1:5,000 in 1% nonfat dry milk in TBS-T. Proteins were visualized using a LI-COR digital imager after incubation with LI-COR anti-rabbit and anti-mouse fluorescently conjugated antibodies (LI-COR Biosciences, no. 926-32213 and no. 926-68022) diluted 1:10,000 in TBS-T supplemented with 1% nonfat dry milk. The amounts of LC3-II, LC3-I and GAPDH were determined by densitometry of scanned films using ImageJ and Fiji.

Automated fluorescence microscopy. Experiments involving neuronal survival analysis and optical pulse imaging used an automated microscopy platform as described[9,25]. Briefly, images were obtained with an inverted microscope (Nikon TE2000) equipped with the PerfectFocus system, a high-numerical aperture 20× objective lens and a 16-bit Andor Clara digital camera with a cooled charge-coupled device. Illumination was provided by a Lambda XL Xenon lamp (Sutter) with a liquid light guide. The ASI 2000 stage was controlled by rotary encoders in all three planes of movement. All of the components were encased in a custom-designed, climate-controlled environmental chamber (InVivo Scientific), kept at 37 °C and 5% CO_2. The Semrock BrightLine full-multiband filter set (DAPI, FITC, TRITC, Cy5) was used for fluorophore photoactivation (DAPI), excitation and detection (FITC, TRITC). The illumination, filter wheels, focusing, stage movements and image acquisitions were fully automated and coordinated with a mix of proprietary (ImagePro) and publicly available (ImageJ and µManager) software.

Image analysis. Relevant data were extracted from the raw, digital images in a sequential process using an original script developed in PipelinePilot (Accelrys, San Diego, CA). Briefly, the median background fluorescence from a portion of all images was calculated and subtracted from each individual image. The images were then assembled into montages representing each well at each time point. The montages were sequenced and aligned automatically, and neuron cell bodies were segmented on the basis of intensity and morphology. Among the variables recorded for each neuron were the fluorescence intensity and the time of death, marked by the loss of cellular fluorescence, rounding or dissolution of the cell body. Neurons with TDP43-Dendra2 intensity values below 20 AU were excluded from half-life analyses. Statistical analyses and the generation of cumulative hazard plots were accomplished using custom-designed algorithms and the survival package within *R*, while scatter plots and bar graphs were created using Prism (GraphPad).

MN culturing and differentiation. iPSCs were generated and characterized as described[32]. Control fibroblasts were obtained from a 56-year-old man and a 40-year-old woman (ATCC), whereas mutant TDP43 fibroblasts were donated from a 56-year-old man. iPSCs were cultured on CF-1 irradiated mouse embryonic fibroblasts with KO-DMEM (Invitrogen) supplemented with 20% knockout serum replacement (Invitrogen), 10 ng/ml basic FGF2 (PeproTech),

doi:10.1038/nchembio.1563

1 mM L-glutamine (Invitrogen), 100 mM 2-mercaptoethanol (Invitrogen), 1% penicillin-streptomycin (Invitrogen) and 1% nonessential amino acids. Before differentiation, cells were resuspended in MTESR1 medium (Stem Cell Technologies) and passaged three times. Neural precursor cells (NPCs) were generated by dual-SMAD inhibition in medium supplemented with SB431542 (10 μM; Tocris), dorsomorphin (2.5 μM; Calbiochem) and *N*-acetylcysteine (0.5 μM; Sigma) for 5–7 d. Cells were dissociated with Accutase (Sigma) and caudalized using retinoic acid (0.1 μM; Sigma) for 7–12 d and then dissociated again and plated onto coverslips coated with laminin (Sigma) and fibronectin (Sigma) in Neurobasal medium (Invitrogen) supplemented with 0.1 μM retinoic acid, 1 μM purmorphamine (Calbiochem), 1% N-2 supplement (Invitrogen), 1% nonessential amino acids (Invitrogen), 1% penicillin-streptomycin (Invitrogen), 1% GlutaMAX (Invitrogen) and 5 ng/ml basic FGF. After 7–10 d, MN precursors were transferred to maturation medium consisting of Neurobasal medium (Invitrogen) supplemented with 0.5% N-2 supplement (Invitrogen), 1% nonessential amino acids (Invitrogen), 1% penicillin-streptomycin (Invitrogen), 0.5% GlutaMAX (Invitrogen), 10 ng/ml brain-derived neurotrophic factor (BDNF; PeproTech), 10 ng/ml glial cell-derived neurotrophic factor (PeproTech) and 10 μM forskolin (Tocris). 2–4 weeks later, neurospheres were dissociated with papain (Worthington) and immediately electroporated using Neon (Invitrogen) with HB9::GFP or MAP2::mApple before plating at 75×10^3 cells per well of a 96-well plate that had been coated with polyornithine (Sigma) and laminin (Sigma).

Astrocyte culturing and differentiation. Astrocytes were differentiated from iPSCs as described[37]. Briefly, NPCs were cultured in DMEM/F12 (Invitrogen) supplemented with 1% N2 (Invitrogen), 0.1% B27 (Invitrogen), 1% non-essential amino acids (Invitrogen), 1% penicillin-streptomycin (Invitrogen), 1% GlutaMAX solution (Invitrogen), 20 ng/ml LIF (Sigma) and 20 ng/ml EGF (R&D Systems) for 4–6 weeks. Spheres were then transferred to DMEM/F12 supplemented with 1% N2, 0.1 % B27, 1% nonessential amino acids, 1% penicillin/streptomycin, 1% GlutaMAX, 20 ng/ml FGF-2 (PeproTech) and 20 ng/ml EGF (R&D Systems) and were mechanically passaged every 2 weeks. To generate monolayer cultures, spheres were dissociated with papain (Worthington Biochemical) and plated in wells coated with Matrigel (BD Biosciences, 1:80). Monolayers were split with Accutase (Sigma) approximately every 3–4 d, or when confluent. Differentiated astrocytes were created by culturing the cells in Neurobasal medium (Invitrogen) supplemented with 0.2% B27, 1% nonessential amino acids, 1% penicillin/streptomycin, 1% GlutaMAX solution and 10 ng/ml CNTF (R&D Systems) for 2 weeks. Before survival analysis, astrocytes were dissociated with Accutase and cultured at a density of 2×10^4 cells per well of a 96-well plate. 2–3 d later, differentiated astrocyte cultures were transfected with pGW1-mApple using Lipofectamine 2000 as described above.

Immunocytochemistry. Cortical neurons from rats were isolated as described[50] and plated onto 12-mm glass coverslips coated with laminin (BD Biosciences) and poly-D-lysine (Millipore), then transfected at 4 d *in vitro* with pGW1-mApple and pGW1-TDP43(WT)-EGFP or pGW1-TDP43^{A315T}-EGFP. Immunocytochemistry was performed as described[50] using rabbit anti-TDP43 polyclonal antibodies (Proteintech, no. 10782-2-AP; 1:1,000) and anti-rabbit Cy5-labeled secondary antibodies (Jackson Immunochemical, no. 711-175-152; 1:250). For LC3 immunocytochemistry, neurons were treated for 24 h at 37 °C with vehicle, NCP, MTM or FPZ, and then fixed and probed with rabbit anti-LC3 primary antibodies (Novus Biologicals, NB100-2331;1:200) and anti-rabbit Alexa 488–labeled secondary antibodies (Invitrogen, A-11008; 1:500). Nuclei were stained by a brief incubation in PBS supplemented with Hoechst dye (Life Technologies, H3569; 10 μM final concentration). Immunocytochemical samples were imaged using a Zeiss LSM510 confocal microscope equipped with Meta. The total normalized TDP43 level was determined by comparing the intensity of TDP43 immunolabeling in transfected cells to that in nontransfected cells within the same high-powered (63×) field, using Fiji.

***In silico* drug screen.** The Discovery Studio 2.1 (Accelrys, San Diego, CA) suite of molecular modeling software was used to assemble and screen a three-dimensional database (3DDB) of commercially available and well-characterized compounds. This collection, totaling over one million compounds, represents a broad cross section of chemical space, including all of the marketed drugs and drugs in development. It includes compounds from several drug libraries, including Maybridge (http://www.maybridge.com/), ChemBridge (http://www.chembridge.com/), MicroSource Discovery Systems (http://www.msdiscovery.com/), Sigma-Aldrich (http://www.sigmaaldrich.com/), TimTec Drug Discovery (http://www.timtec.com/), Specs (http://www.specs.com/), ZINC (http://zinc.docking.org/), the World Drug Index (http://thomsonreuters.com/world-drug-index/) and Interbioscreen (http://www.ibscreen.com/). Pharmacophore hypotheses were generated using the two most active compounds in a previously performed screen[22] using the HipHop algorithm within the Pharmacophore Protocol of Discovery Studio to automatically build the common-features pharmacophore models using hydrophobe, hydrophobe aromatic, acceptor, donor and charged positive features. Up to 255 low-energy conformations for each of the compounds (based on the initial low-energy conformation) were included in this analysis. Briefly, the program evaluates chemical features that compounds have in common on the basis of common conformations. The algorithm starts with a small set of features and extends them until no further common conformation of the input compounds is found. Multiple hypotheses are generated and scored. These hypotheses are spatial dispositions of chemical features the input compounds share in common. All three and four feature hypotheses were evaluated using the Ligand Pharmacophore Mapping function and scoring module within the Pharmacophore Protocol of Discovery Studio. The relative concordance of the scoring function was compared to the neuronal autophagy stimulation ranking for each compound, as previously determined[22]. The best three-feature pharmacophore model (two hydrophobic aromatic features and one charged positive feature) was selected and systematically modified with exclusion spheres (ligand inaccessible areas) to properly rank each compound with the computed scoring function. Fourteen exclusion spheres were added to the three-feature pharmacophore model, and this model was used in conjunction with the 3DDB to conduct the *in silico* HTS. Scoring was assessed using a fit function that determined the goodness of fit of each compound to the features of the model. In addition, high-scoring hits from the initial screen were also fit to the 'shape' feature of the model, and the highest-scoring compounds from this filter (MTM and FPZ) were evaluated as described in the text.

Compounds. MTM and FPZ were acquired from Sigma (M4406 and F4765, respectively). The purity of MTM was ≥95%, and that of FPZ was ≥98%, as determined by thin-liquid chromatography and $HClO_4$ titration. NCP was purchased from EMD Millipore (no. 124020), with a purity of ≥95% as measured by high-performance LC. All of the compounds were solubilized in DMSO at 10 mM and stored at −20 °C until just before use.

Statistical analysis. One-way ANOVA with Dunnett's test was used for comparison of multiple means in **Figures 4b,c** and **5a,c,e–i** and **Supplementary Figure 6a**. The two-sided Kolomogorov-Smirnov test was used to determine differences between nonparametric probability distributions in **Figures 1a,b**, **3b–d**, **4g** and **5b,d** and **Supplementary Figures 5a** and **6j**. The Mann-Whitney test was used to compare medians from nonparametric data in **Figure 3a**. The Kruskal-Wallis test with Dunn's post-test was used for comparisons of medians from multiple non-parametric data groups in **Figure 4f**. Linear regression was used in **Figure 1f,g** and **Supplementary Figures 3e** and **4c–e**. First-order exponential decay curve fitting was used to model half-life in **Figures 2b,e,f** and **4e**. Cox proportional hazards analysis was used to determine differences in survival among populations in **Figures 1d,e** and **6a–e**, **Supplementary Figures 2a–e**, **5b** and **7a–c**.

50. Saudou, F., Finkbeiner, S., Devys, D. & Greenberg, M.E. Huntingtin acts in the nucleus to induce apoptosis but death does not correlate with the formation of intranuclear inclusions. *Cell* **95**, 55–66 (1998).

SUPPLEMENTARY INFORMATION

Autophagy induction enhances TDP43 turnover and survival in neuronal ALS models

Sami J. Barmada[1,2,7], Andrea Serio[4], Arpana Arjun[1], Bilada Bilican[4], Aaron Daub[1], D. Michael Ando[1,5], Andrey Tsvetkov[1], Michael Pleiss[6], Xingli Li[7], Daniel Peisach[7], Christopher Shaw[8], Siddharthan Chandran[4], and Steven Finkbeiner[1,2,3,5,6,9]

[1]Gladstone Institute of Neurologic Disease, San Francisco, California, 94158; Departments of Neurology[2] and Physiology[3], University of California, San Francisco, Medical Center, San Francisco, California 94143; [4]Euan MacDonald Centre for Motor Neurone Disease Research, and Medical Research Council Centre for Regenerative Medicine, University of Edinburgh, UK; [5]Biomedical Sciences Graduate Program, University of California, San Francisco, California 94158; [6]Keck Program in Brain Cell Engineering, Gladstone Institutes, San Francisco, California, 94158; [7]Department of Neurology, University of Michigan, Ann Arbor, MI 48109; [8]Institute of Psychiatry, Medical Research Council Centre for Neurodegeneration Research, King's College London, London, UK; [8]Taube-Koret Center for Neurodegenerative Disease Research, Hellman Family Foundation Alzheimer's Disease Research Program, and Roddenberry Stem Cell Program, San Francisco, California 94158.

Correspondence should be addressed to Steven Finkbeiner, The Gladstone Institutes, 1650 Owens Street, San Francisco, CA 94158, Tel: (415) 734-2508, Fax: (415) 355-0824, Email: sfinkbeiner@gladstone.ucsf.edu.

SUPPLEMENTARY RESULTS

Supplementary Figure 1: Automated microscopy of primary neurons expressing TDP43-EGFP. Most neurons displayed nuclear localization of TDP43-EGFP (a–d), but a significant fraction exhibited cytoplasmic mislocalization (e–h) and/or cytoplasmic aggregates of TDP43-EGFP (i–l). (a, e, i) mApple; (b, f, j) TDP43-EGFP; (c, g, k) Hoechst nuclear stain; (d, h, l) merged images. Scale bar = 25 μM.

Supplementary Figure 2: The survival of control neurons is unaffected by the amount of transfected EGFP or autophagy inducers at low doses. Primary rat cortical neurons were dissected, cultured, and transfected with mApple and EGFP, then imaged using automated fluorescence microscopy. (a) The amount of EGFP DNA did not affect the survival of transfected neurons (0.13 ng/μl, n=317, reference group; 0.27 ng/μl, n=330; 0.54 ng/μl, n=327; 0.67 ng/μl, n=325). Data were pooled from 8 wells per condition, performed in duplicate. (b) Neurons expressing EGFP were unaffected by treatment with 0.5 μM of NCP, MTM, or FPZ (DMSO, n=480, reference group; NCP, n=211; MTM, n=262; FPZ, n=267). Data were combined from eight wells per condition in each of five experiments. (c) At higher doses, NCP causes significant toxicity in control primary neurons expressing only EGFP. (DMSO, n=126, reference group; 0.5 μM NCP, n=113 neurons; 1.5 μM NCP, n=112 neurons, HR=1.61; 2.5 μM NCP, n=64 neurons, HR=1.81). In contrast, neither MTM (d) nor FPZ (e) had significant effects upon survival at doses up to 2.5 μM. (For panel d, DMSO, n=96, reference group; 0.5 μM MTM, n=82 neurons; 1.5 μM MTM, n=109 neurons; 2.5 μM MTM, n=78 neurons. For panel e, DMSO, n=245, reference group; 0.5 μM FPZ, n=256 neurons; 1.5 μM FPZ, n=236 neurons; 2.5 μM FPZ, n=225 neurons.) Data combined from eight wells per condition, in duplicate. *$p < 0.01$; ns, not significant ($p > 0.05$) by Cox proportional hazards analysis.

Supplementary Figure 3: Determining the "dose" of exogenous TDP43 in transfected neurons. Primary neurons were isolated, cultured, and transfected with TDP43-EGFP and mApple. At 24 h after transfection, immunocytochemistry was used to determine the total amount of TDP43 within transfected neurons. (a-d) Micrographs of neurons transfected with TDP43-EGFP (a) and mApple (c), stained with anti-TDP43 antibodies (b) and Hoechst dye (d). The intensity of TDP43 in untransfected neurons (arrowheads, b) was used as a reference to calculate the amount of total TDP43 in transfected neurons (arrows, b). Scale bar = 10 μm. (e) Plot depicting the relation between the concentration of TDP43(WT)-EGFP (blue) or TDP43(A315T)-EGFP (red) DNA and total normalized TDP43. By linear regression, the total normalized TDP43 is $5.4x_{WT} + 1.1 \pm 0.5$ for TDP43(WT)-EGFP ($R^2 = 0.9105$), and $4.1x_{A315T} + 1.4 \pm 0.3$ for TDP43(A315T)-EGFP ($R^2 = 0.9450$), where x_{WT} is the concentration of TDP43(WT)-EGFP DNA (ng/μl), and x_{A315T} is the concentration of TDP43(A315T)-EGFP DNA (ng/μl). Error bars represent ± SEM. (f) Downregulation of endogenous TDP43 by exogenous TDP43-EGFP. Primary neurons were transfected with vector DNA encoding TDP43(WT)-EGFP or TDP43(A315T)-EGFP at the indicated concentrations, and the

amount of TDP43 determined by quantitative immunocytochemistry. Downregulation of endogenous TDP43 is apparent in cells with a fold endogenous TDP43 < 1. Horizontal bars indicate mean fold endogenous TDP43 levels for each condition. Values were pooled from 17–30 neurons per condition, performed in duplicate.

Supplementary Figure 4: Complementary methods for measuring neuronal TDP43 turnover. (a) Representative, full-length autoradiographic exposures of immunoprecipitated material from metabolically labeled rodent primary cortical neurons. TDP43 was immunoprecipitated at 0, 5, 15, or 25 h after pulse labeling by (1) anti-TDP43 antibodies from ThermoScientific (PA5-17011), (2) anti-TDP43 antibodies from G. Yu and J. Herz (University of Texas, Southwestern), or control anti-IgG antibodies. * denotes full-length TDP43. Molecular weight in kDa is shown to the left of each gel. (b) Schematic diagram comparing metabolic pulse chase (MPC, top) with optical pulse labeling (OPL, bottom). (c-e) Half-life values for individual cells expressing TDP43(WT)-Dendra2 (c), TDP43(A315T)-Dendra2 (d), or Dendra2 (e) were plotted against the normalized RFP intensity immediately after photoconversion. By linear regression, there was no significant relationship between half-life and expression level for any of the constructs. TDP43(WT)-Dendra2, n=207, R^2 = 0.0039. TDP43(A315T)-Dendra2, n=251, R^2 = 0.0108; Dendra2, n=546, R^2 = 0.0052. Values were pooled from 8–12 wells per construct, and five independent experiments. Dotted lines represent 95% confidence intervals.

Supplementary Figure 5: ALS-associated TDP43(M337V). (a) Probability density plot of single-cell half-life measurements from neurons expressing TDP43(WT)-Dendra2 (cyan, n=128) and TDP43(M337V)-Dendra2 (green, n=111), demonstrating a higher probability of observing a low TDP43-Dendra2 half-life in neurons expressing TDP43(M337V)-Dendra2. * $p=1.6\times10^{-4}$, two-sided Kolmogorov-Smirnov test). Values were obtained from eight wells per condition, performed in duplicate. (b) FPZ lowered the risk of death in neurons expressing TDP43(M337V)-EGFP. By Cox proportional hazards analysis, for TDP43(M337V)-EGFP + DMSO vs EGFP, HR=1.49, ** $p=6.2\times10^{13}$; for TDP43(M337V)-EGFP + FPZ vs EGFP, HR=1.17, * p=0.006; and for TDP43(M337V)-EGFP + DMSO vs TDP43(M337V)-EGFP + FPZ , HR=0.78, $p=1.7\times10^{6}$. EGFP, n=851; TDP43(M337V)-EGFP + DMSO, n=914; TDP43(M337V)-EGFP + FPZ, n=931. Data were pooled from 8–12 wells per condition, performed in duplicate.

Supplementary Figure 6: Small-molecule autophagy inducers effectively stimulate autophagic flux in primary neurons. (a) Primary neurons were treated for 24 h with the indicated autophagy inducer at 0.5 or 5.0 μM, then analyzed by SDS-PAGE and western blotting using anti-GAPDH antibodies (left) or anti-LC3 antibodies (right). ♦, GAPDH; *, LC3-I; **, LC3-II. (b) Autophagic induction by small molecules in the presence of NH_4Cl. Primary neurons were incubated with vehicle or drug (5 μM) for 24 h, and NH_4Cl (50 mM) for 6 h before lysis, SDS-PAGE, and western blotting for LC3. * $p < 0.05$; ns, $p > 0.05$, by one-way ANOVA with Dunnett's test. Values were pooled from 9 independent experiments. (c-i) LC3 immunocytochemistry, demonstrating the formation of large LC3-positive puncta in primary neurons treated with 5 μM but not 0.5 μM of each compound. Scale bar = 10 μM. (j) FPZ, MTM and NCP fail to increase LC3-

Dendra2 turnover in the absence of ATG7, a critical component of autophagy. Primary neurons were co-transfected with LC3-Dendra2 and shRNA directed against *ATG7* (KD-ATG7) or scrambled shRNA (Sc), photoactivated, and half-life calculated from cell intensities measured by automated microscopy. Half-life was then plotted using a probability density function. Sc + DMSO, n=917 neurons; Sc + FPZ, n=262 neurons; Sc + MTM, n=665 neurons; Sc + NCP, n=666 neurons; KD-ATG7 + DMSO, n=917 neurons; KD-ATG7 + FPZ, n=273 neurons; KD-ATG7 + FPZ, n=695 neurons; KD-ATG7 + NCP, n=698 neurons. Sc + DMSO *vs.* KD-ATG7 + DMSO, * $p < 0.05$ for right-shift in curve; KD-ATG7 + DMSO *vs.* KD-ATG7 + FPZ, ns ($p > 0.05$); KD-ATG7 + DMSO *vs.* KD-ATG7 + MTM, ‡ $p < 0.05$ for right-shift in curve; KD-ATG7 + DMSO *vs.* KD-ATG7 + NCP, ns ($p > 0.05$). All comparisons by two-sided Kolmogorov-Smirnov test. Data were pooled from 8-12 wells per condition, performed in duplicate.

Supplementary Figure 7: Autophagic induction does not affect the survival of WT human iPSC-derived neurons and astrocytes. Human iPSCs carrying WT TDP43 were differentiated into motor neurons or astrocytes, treated with 0.5 μM MTM, FPZ, or vehicle control, then followed by longitudinal fluorescence microscopy. (a) Autophagy inducers did not significantly affect the survival of WT human iPSC-derived motor neurons expressing HB9::GFP (ns, $p > 0.05$ by Cox proportional hazards analysis. DMSO, n=11; FPZ, n=40; MTM, n=40). Data were pooled from 8-12 wells per condition, performed in triplicate. (b) There was no significant effect of autophagy inducers on the survival of WT human iPSC–derived neurons expressing MAP2::mApple (ns, $p > 0.05$ by Cox proportional hazards analysis. DMSO, n=112; FPZ, n=131; MTM, n=138). Data were pooled from 8–12 wells per condition, performed in triplicate. (c) Autophagy inducers also failed to significantly affect survival in WT human iPSC-derived astrocytes (ns, $p > 0.05$ by Cox proportional hazards analysis. DMSO, n=127; FPZ, n=208; MTM, n=131). Results were combined from 8–12 wells per condition, performed in duplicate.

Supplementary Table 1: Cox proportional hazards analysis of TDP43-EGFP in primary rodent cortical neurons.

	DNA (ng/μl)	N	HR	95% CI	p[†]
TDP43(WT)-EGFP	0.13	290	1.56	1.31–1.86	6.2×10^{-7}
	0.27	334	1.69	1.43–2.01	2.2×10^{-9}
	0.54	321	2.56	2.16–3.04	$<2\times10^{-16}$
	0.67	342	2.98	2.51–3.53	$<2\times10^{-16}$
TDP43(A315T)-EGFP	0.13	315	1.28	1.08–1.54	5.6×10^{-3}
	0.27	332	1.89	1.60–2.25	2.9×10^{-13}
	0.54	319	2.63	2.22–3.13	$<2\times10^{-16}$
	0.67	324	2.99	2.52–3.55	$<2\times10^{-16}$

N, number of neurons per group. HR, hazard ratio, with EGFP (0.13 ng/μl) as the reference group. CI, confidence interval. [†] The minimum p value for this assay is 2×10^{-16}.

Supplementary Table 2: Effect of small-molecule autophagy inducers on the risk of death in primary neurons expressing TDP43-EGFP.

	Drug (0.5 μM)	N	HR	95% CI	p[†]
EGFP	DMSO	480	Ref	–	–
TDP43(WT)-EGFP	DMSO	347	1.90	1.56–2.25	1.1×10^{-11}
	FPZ	143	1.22	0.93–1.60	0.15
	MTM	132	1.40	1.07–1.83	0.01
	NCP	160	1.70	1.33–2.16	1.8×10^{-5}
TDP43(A315T)-EGFP	DMSO	331	1.77	1.47–2.14	3.4×10^{-9}
	FPZ	200	1.07	0.84–1.35	0.60
	MTM	248	1.28	1.03–1.59	0.02
	NCP	193	1.51	1.19–1.90	5.6×10^{4}

N, number of neurons per group. HR, hazard ratio, with EGFP + vehicle (DMSO) as the reference group (Ref). CI, confidence interval. In Fig. 6a, ns, $p > 0.05$; *** $p=1\times10^{-11}$; ** $p=2\times10^{-5}$; * $p=0.01$. In Fig. 6b, ns $p > 0.05$; *** $p=3\times10^{-9}$; ** $p=6\times10^{-4}$; * $p=0.02$. All p values determined by Cox proportional hazards analysis. [†] The minimum p value for this assay is 2×10^{-16}.

Supplementary Table 3: Effect of small molecule autophagy inducers on the risk of death in iPSC-derived neurons and astrocytes.

		Drug (0.5 μM)	N	HR	95% CI	p[†]
HB9+ neurons	**WT**	DMSO	11	Ref	–	–
	M337V	DMSO	33	2.64	1.02–6.82	0.04
		FPZ	86	1.45	0.57–3.68	0.43
		MTM	64	1.70	0.66–4.34	0.27
MAP2+ neurons	**WT**	DMSO	112	Ref	–	–
	M337V	DMSO	133	1.44	1.05–1.97	0.02
		FPZ	116	1.12	0.79–1.59	0.51
		MTM	150	0.91	0.66–1.27	0.59
Astrocytes	**WT**	DMSO	127	Ref	–	–
	M337V	DMSO	147	2.53	1.93-3.33	2.5×10^{-11}
		FPZ	139	1.64	1.24-2.18	5.2×10^{-4}
		MTM	125	1.51	1.12-2.01	6.1×10^{-3}

N, number of neurons per group. HR, hazard ratio, with WT + vehicle as the reference group (Ref). CI, confidence interval. In Figure 6c and d, ns $p > 0.05$; * $p=0.02$. In Fig. 6e, *** $p=2\times10^{-11}$; ** $p=5.2\times10^{4}$; * $p=6.1\times10^{-3}$. All p values determined by Cox proportional hazards analysis. [†] The minimum p value for this assay is 2×10^{-16}.

Supplementary Figure 1

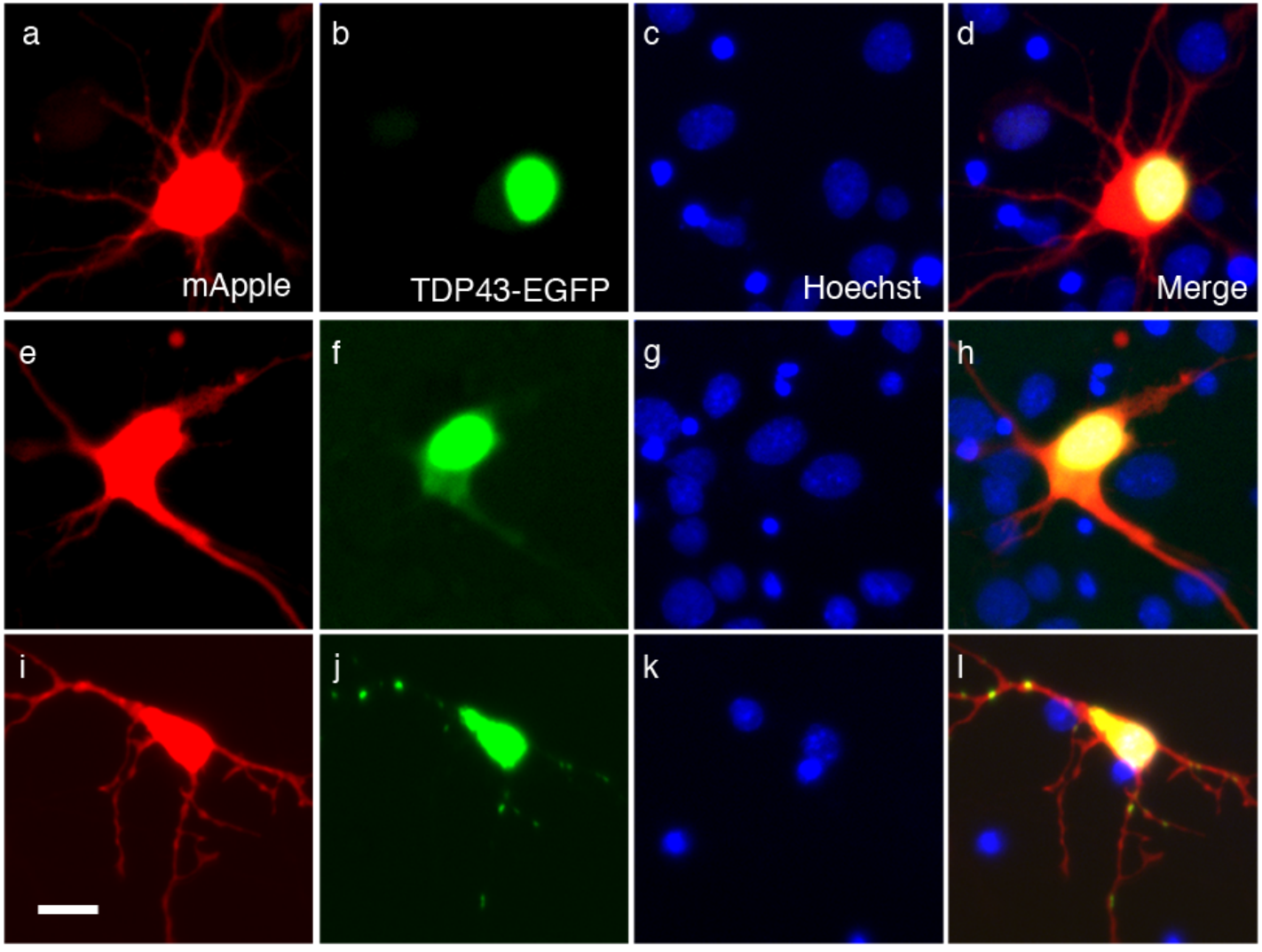

Nature Chemical Biology: doi:10.1038/nchembio.1563

Supplementary Figure 2

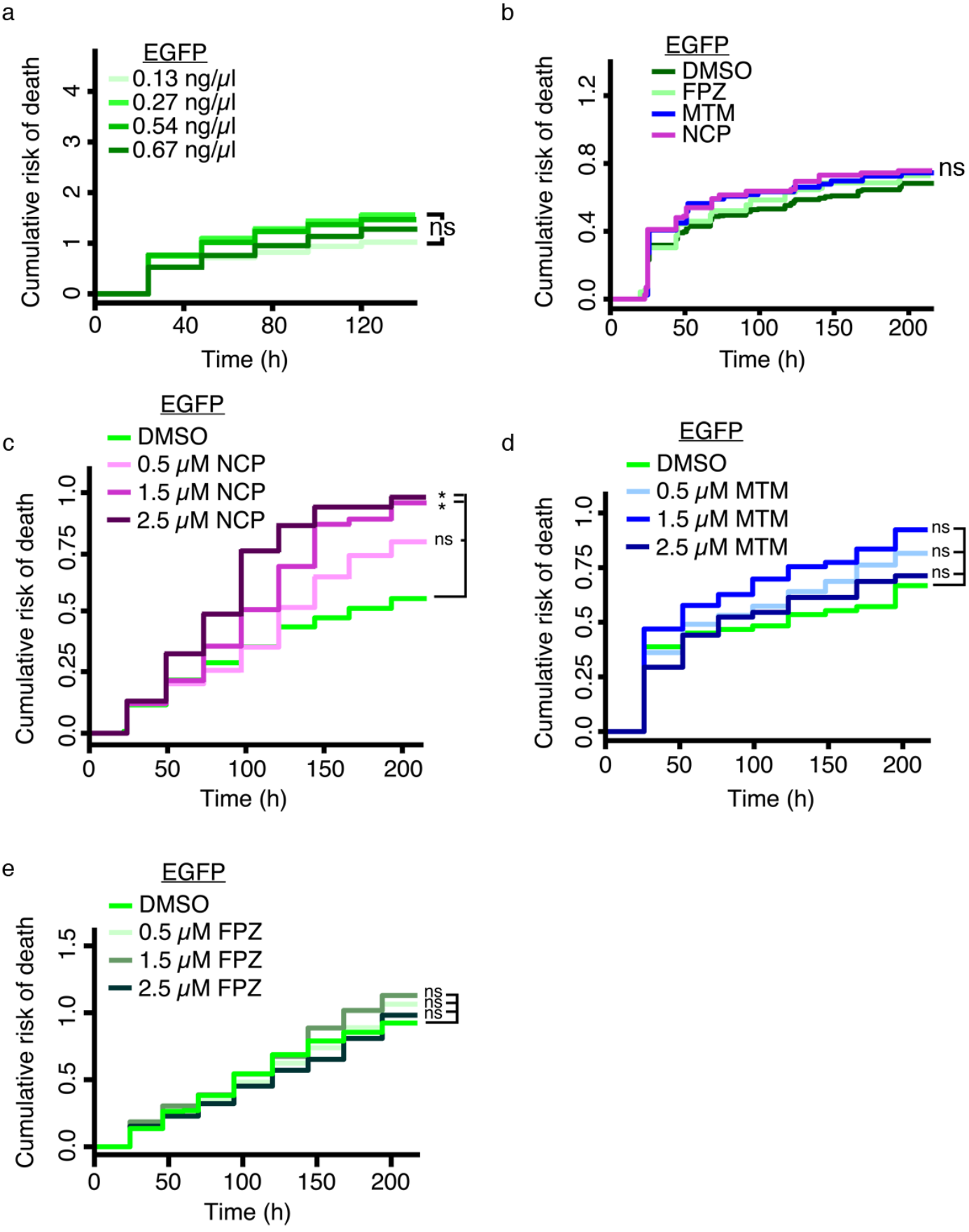

Supplementary Figure 3

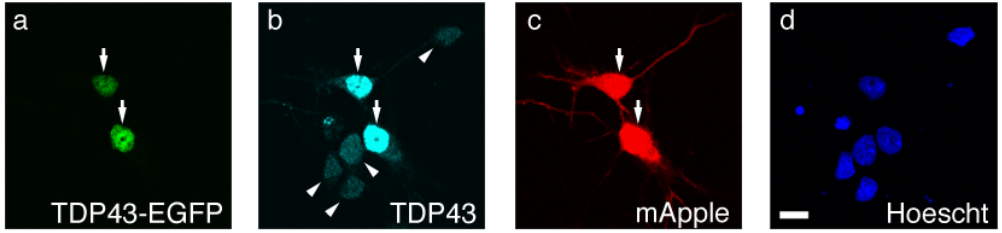

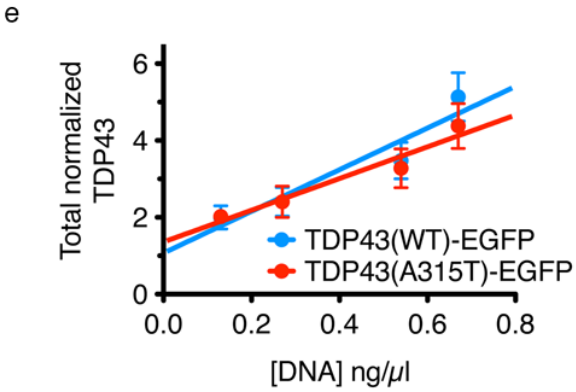

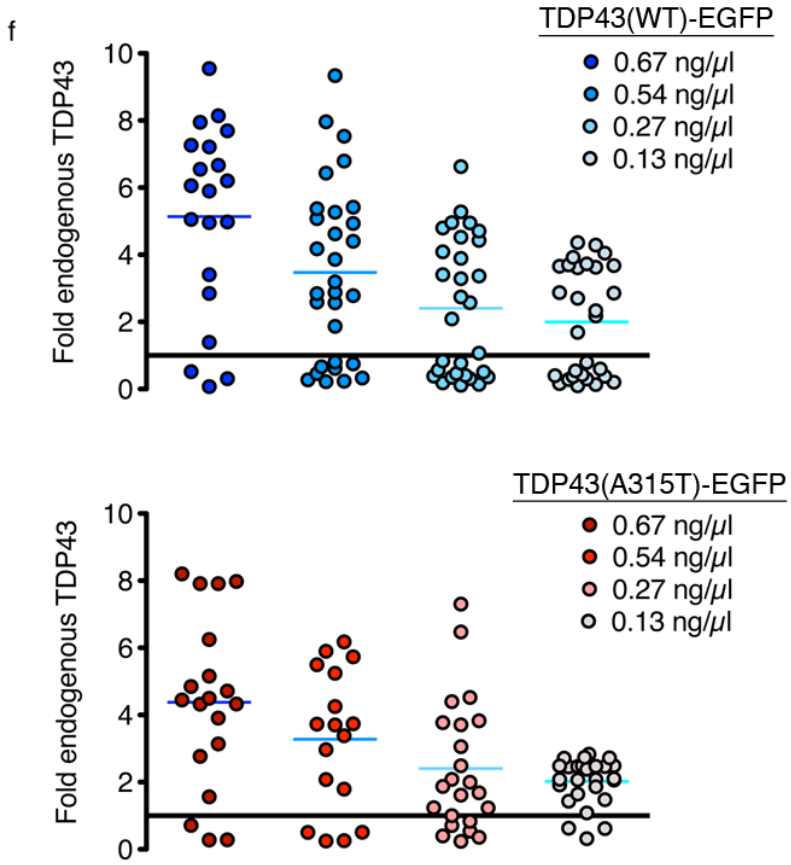

Nature Chemical Biology: doi:10.1038/nchembio.1563

Supplementary Figure 4

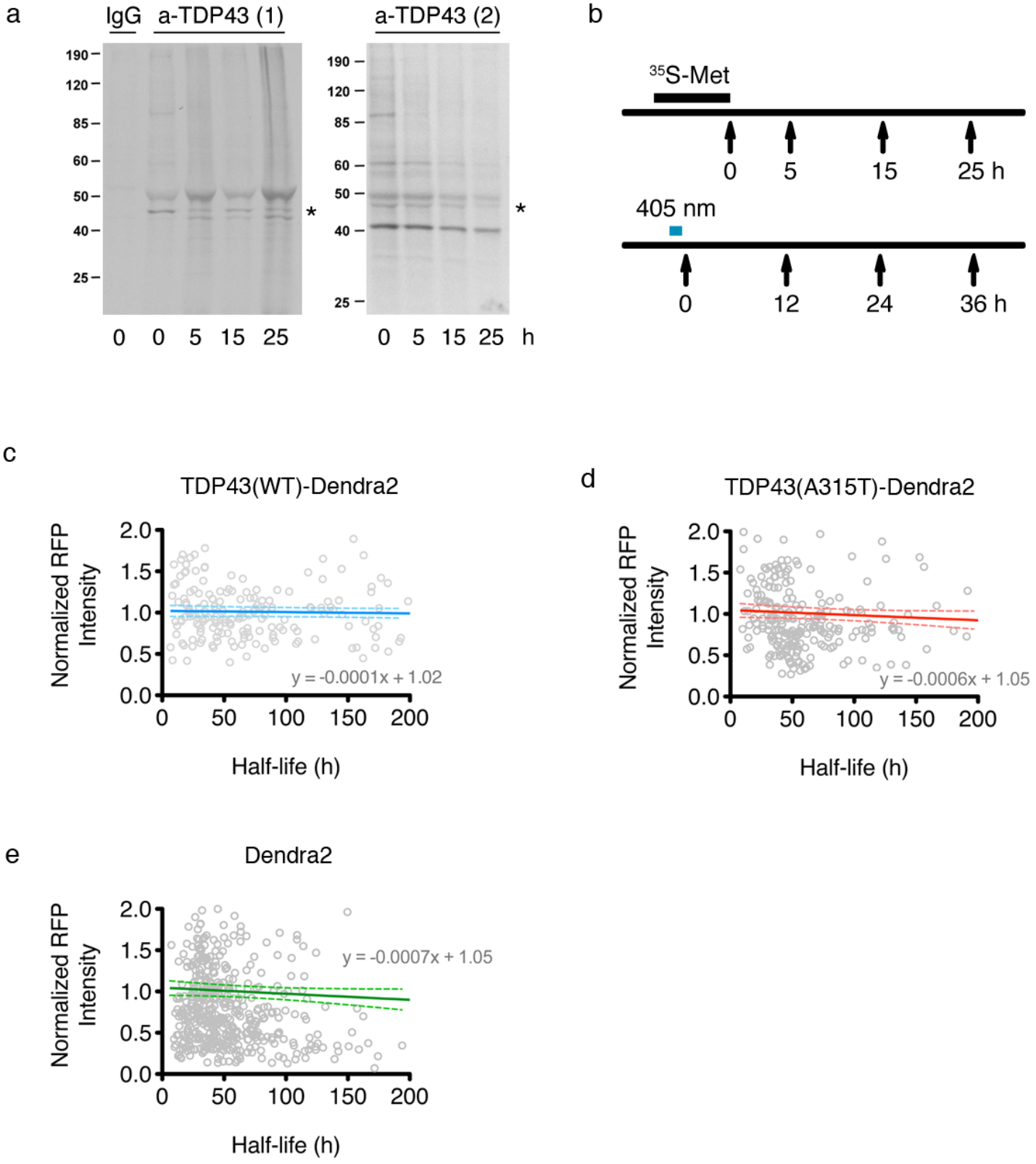

Supplementary Figure 5

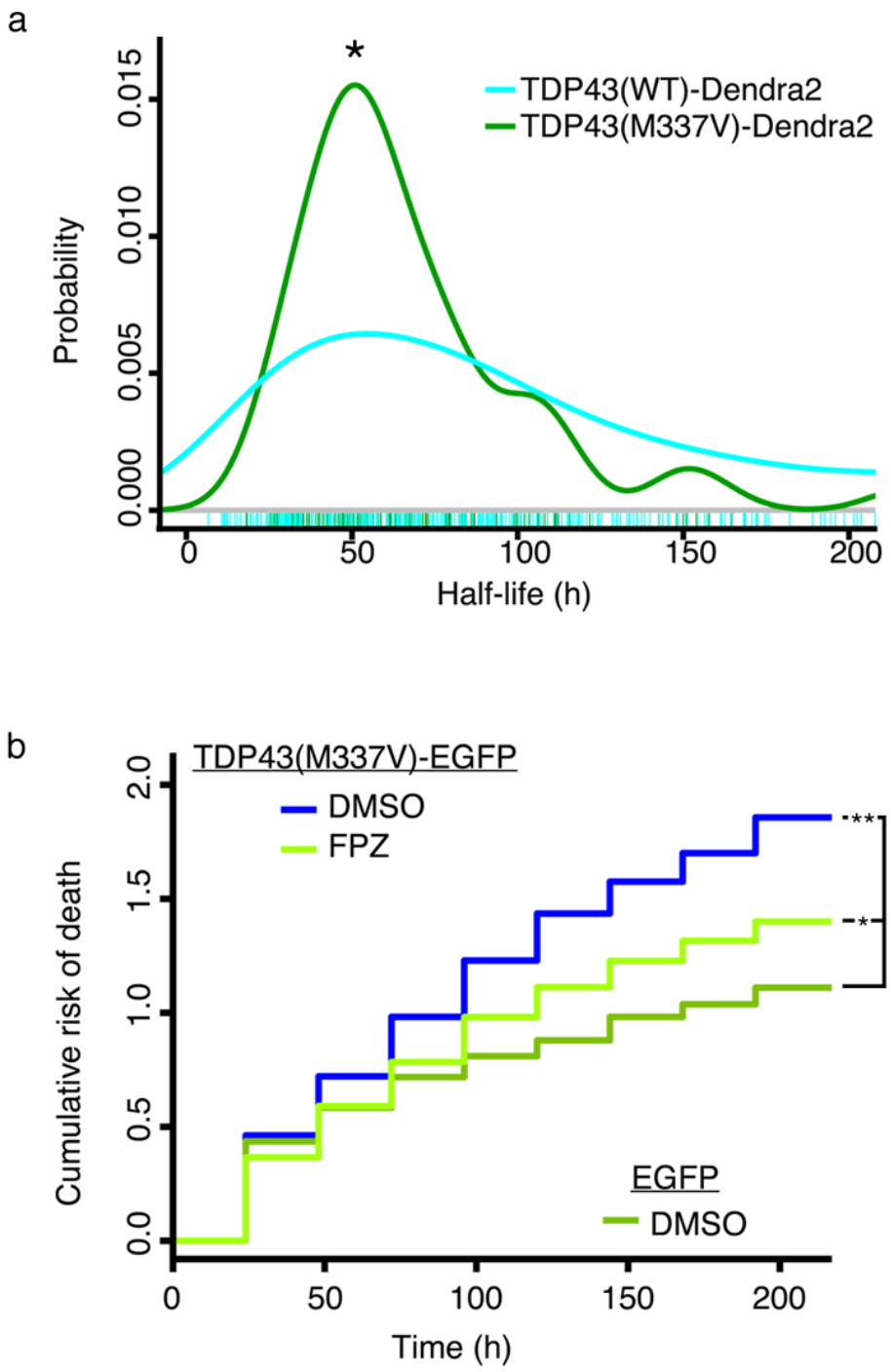

Supplementary Figure 6

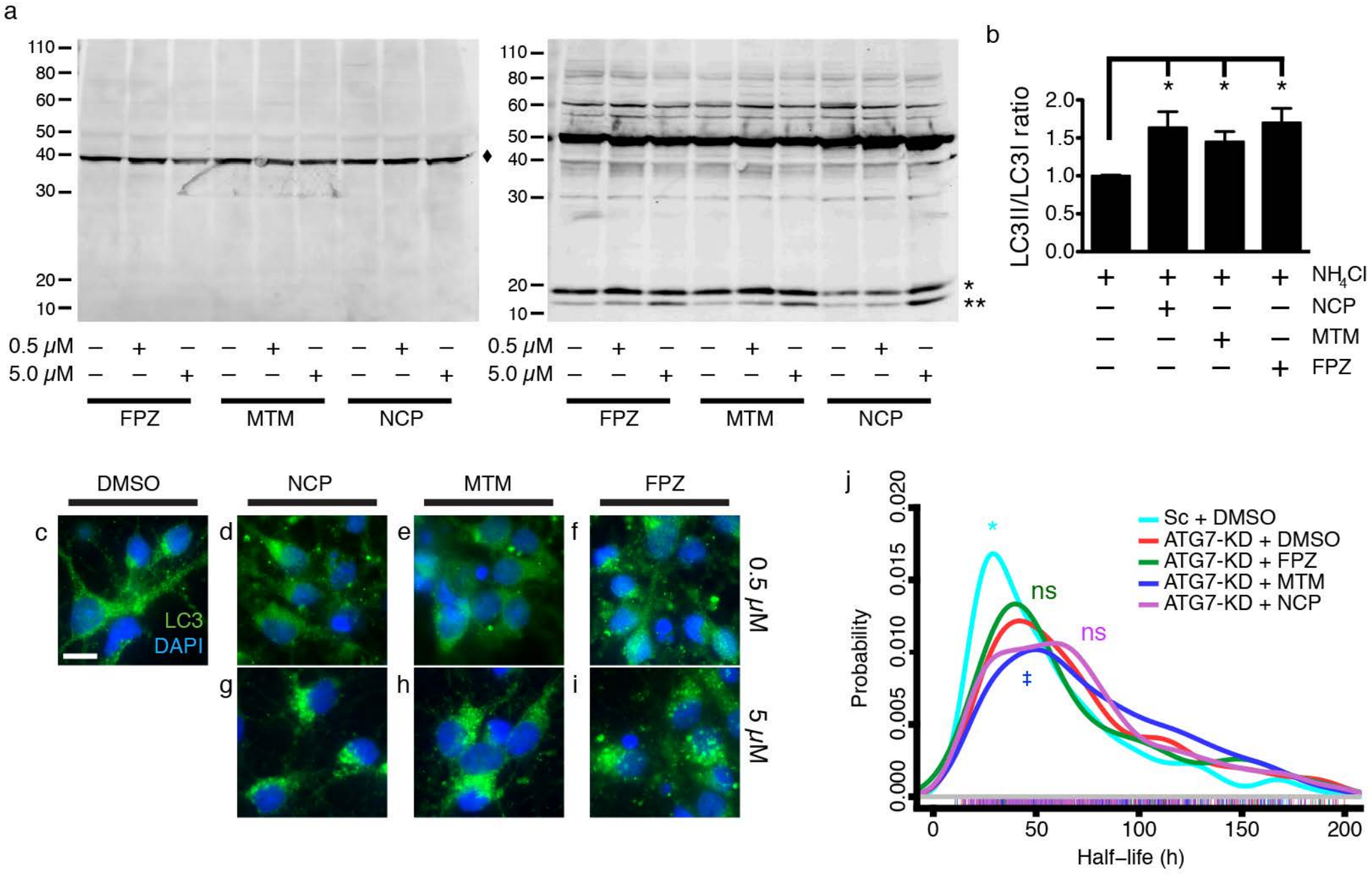

Nature Chemical Biology: doi:10.1038/nchembio.1563

Supplementary Figure 7

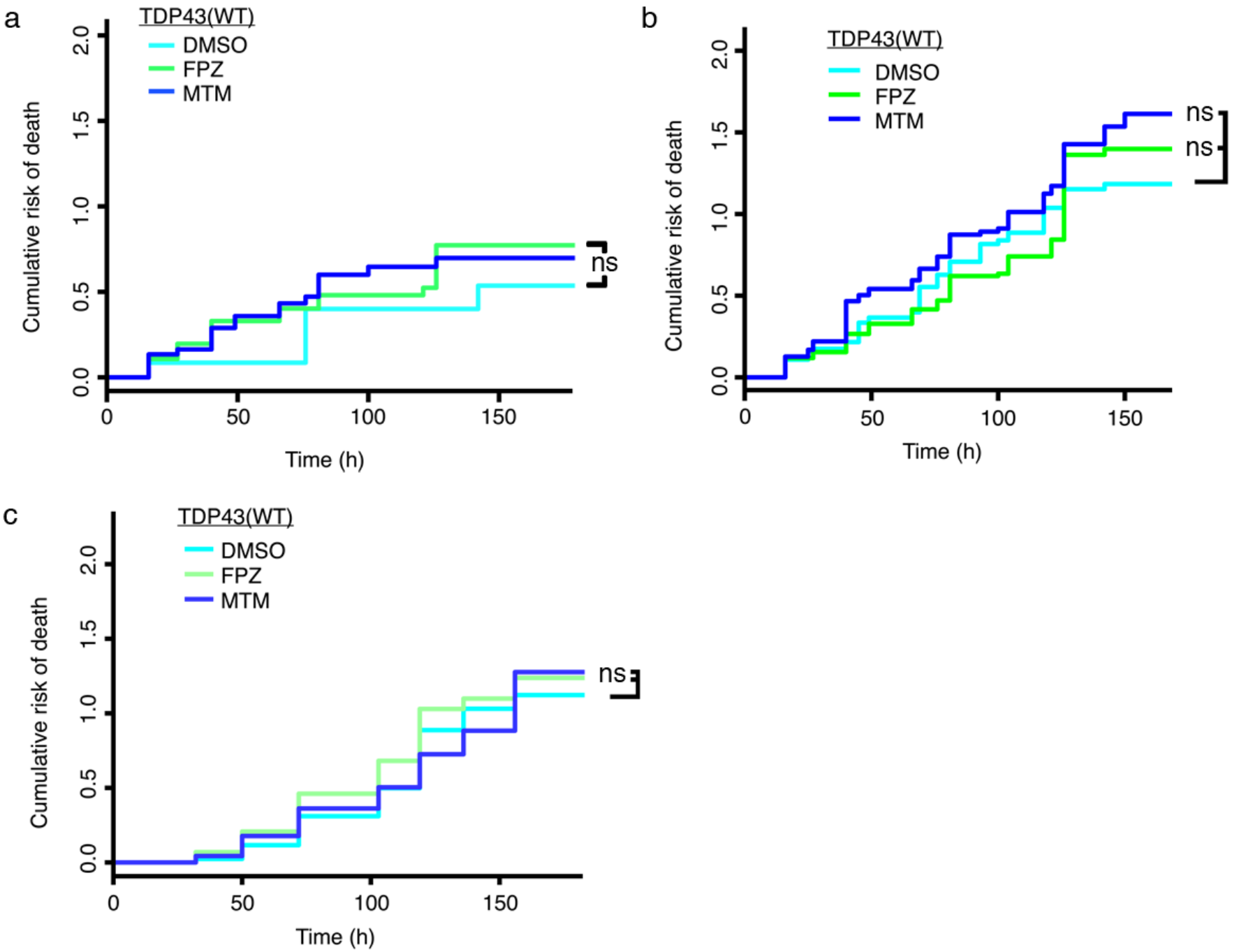

Nature Chemical Biology: doi:10.1038/nchembio.1563